

Modeling, Simulation, and Fabrication
of a PZT Valveless Micropump

by

Shifeng Li

A thesis submitted to the graduate faculty
in partial fulfillment of the requirements for the degree of
MASTER OF SCIENCE

Major: Industrial Engineering

Program of Study Committee:
Shaochen Chen, Major Professor
Li Cao
Ranga Narayanaswami

Iowa State University

Ames, Iowa

2001

Copyright © Shifeng Li, 2001. All rights reserved.

Graduate College
Iowa State University

This is to certify that the Master's thesis of
Shifeng Li
has met the thesis requirements of Iowa State University

Signatures have been redacted for privacy

Dedicated to my wife Rong and my Parents

TABLE OF CONTENTS

LIST OF FIGURES	vi
LIST OF TABLES	viii
NOMENCLATURE	ix
ACKNOWLEDGEMENTS	xi
ABSTRACT	xii
CHAPTER 1. INTRODUCTION	1
1.1 Micro Total Analysis System	1
1.2 Micropump and Valve	3
1.2.1 Micro actuator	4
1.2.2 Micro valve	7
1.2.2.1 Active micro valve	7
1.2.2.2 Passive micro valve	9
1.2.3 Micropump	10
1.2.3.1 Reciprocating type Micropump	11
1.2.3.2 Peristaltic type Micropump	12
1.3 Valveless Micropump	14
1.4 Thesis Organization	16
CHAPTER 2. MODELING OF PZT VALVELESS MICROPUMP	18
2.1 Principle of Valveless Micropump	18
2.1.1 Diffuser Element Analysis	18

2.1.2 Nozzle Element Analysis	23
2.2 Working Principle of Valveless Micropump	26
2.3 Modeling of PZT Valveless Micropump	29
2.3.1 Modeling of PZT Micropump membrane	29
2.3.2 Conservation of Mass and Coupling of PZT and Fluid	33
2.3.3 Dynamic Equation about Nozzle (Extended Bernoulli Equation)	36
CHAPTER 3. SIMULATION OF VALVELESS MICROPUMP	38
3.1 Algorithm of Simulation	38
3.2. Simulation Results and Discussions	39
3.2.1 Membrane Dimensions Effect on Flowrate and Backpressure	39
3.2.2 Nozzle Dimensions Effect on Flowrate and Backpressure	42
3.3 Optimized Micropump	46
3.4 Performances in High Frequency Domain	48
CHAPTER 4. FABRICATION OF VALVELESS MICROPUMP	49
4.1 Mask Design of Valveless Micropump	49
4.2 Fabrication of Valveless Micropump	50
4.3 Fabrication Problem Analysis	55
4.3.1 350 °C PECVD Nitride KOH etching strip	55
4.3.2 4000 A low stress Nitride KOH etching strip	57
CHAPTER 5. CONCLUSIONS	59
5.1 Conclusions of present works	59
5.2 Recommendation for future works	60

REFERENCES

61

LIST OF FIGURES

Figure 1.1 Schematics of the passive Microvalve

Figure 2.1 Diffuser Element Section View

Figure 2.2 Diffuser flow in the positive direction

Figure 2.3 Diffuser flow in the negative direction

Figure 2.4 Nozzle Element Section View

Figure 2.5 PZT Valveless Micropump

Figure 2.6 Valveless Micropump Supply Working Mode

Figure 2.7 Valveless Micropump Pumping Working Mode

Figure 2.8 Membrane Plate Force View

Figure 2.9 Plate deformation under uniform pressure p

Figure 2.10. Pump Chamber Control Volume

Figure 3.1 Flow rates at different membrane thickness and membrane radius

Figure 3.2 Backpressure at different membrane thickness and membrane radius

Figure 3.3 Effect of Nozzle Neck dimension on backpressure

Figure 3.4 Effect of Nozzle Length on backpressure

Figure 3.5 Effect of Nozzle Neck Dimension on Flow Rate

Figure 3.6 Effect of Nozzle Length on Flow Rate

Figure 3.7 Optimized Micropump Inlet and Outlet Flow Rate

Figure 3.8 Optimized Micropump Working Characteristics

Figure 4.1 PECVD nitride strip

Figure 4.2 4000 Å thickness low stress nitride strips away after 6 hours KOH etching

LIST OF TABLES

Table 1.1	Features of the miniaturized conventional Microactuators
Table 1.2	Summation of all kind of Micropump performances
Table 2.1	Summarization of flow efficiency of different nozzle and diffuser elements

NOMENCLATURE

K	loss coefficient
P	pressure Pa
V	chamber volume
V _{gas}	trapped gas volume
V ₀	trapped gas volume at atmosphere
A	nozzle section area m ³
S	flow path section length micron
A _{neck}	neck section area m ³
A _{upsteam}	neck upstream area m ³
A _{in}	inlet section area m ³
A _{out}	outlet section area m ³
C _p	pressure recovery coefficient
L	nozzle length micron
E ₃	PZT electrical density V/m ²
U	PZT applied voltage V
t	time s
H _f	plate thickness micron
H _d	bonding material thickness
M	moment Nm
d ₃₁	strain coefficient 1.8e-10 m/v
d ₃₃	strain coefficient 3.6e-10m/v
C ₁₃	coupling coefficient 0.35

C_{33}	coupling coefficient 0.69
e_{13}	voltage coefficient 0.011 Vm/N
e_{33}	voltage coefficient 0.025 Vm/N
D	passive plate stiffness Nm
a	radius of passive plate micron
r	radius of passive plate micron
W_1	displacement induced by PZT micron
W_2	displacement induced by pressure inside chamber micron
Z_{in}	potential height of inlet micron
Z_{out}	potential height of outlet micron
g	gravity accelerate 9.8N/kg
P_{in}	inlet pressure Pa
P_{out}	outlet pressure Pa
P_0	atmosphere pressure 1.01 KPa
H	wafer thickness micron

Greek letters

ρ_{liquid}	fluid density $1.0 \times 10^3 \text{ kg/m}^3$
ρ_{gas}	trapped gas density kg/m^3
u	upstream mean velocity m/s
α	diffuser/nozzle angle $^\circ$
ξ	pressure loss coefficient
η	coefficient ratio
ϕ_{in}	inlet flow rate ml^3/min

ϕ_{out}	outlet flow rate ml ³ /min
ϵ_x	plane strain in the x direction m
ϵ_y	plane strain in the y direction m
ϵ_z	plane strain in the z direction m
σ_x	plane stress in the x direction Pa
σ_y	plane stress in the y direction Pa
σ_z	plane stress in the z direction Pa
γ	Poisson ratio

Acronyms

SMA	shape memory alloy
PZT	lead zirconate titanate
MEMS	Micro Electro Mechanical Systems
LPCVD	low pressure chemical vaporization deposition
PECVD	plasma enhanced chemical vaporization deposition
STS	Surface Technology Systems
PR	photo resist
KOH	Potassium hydroxide
DRIE	deep reactive ion etching
uTAS	Micro/Miniaturized Total Analysis System

ACKNOWLEDGEMENTS

First and foremost, it is my great pleasure to express my heartfelt appreciation and gratitude to my major professor, Dr. ShaoChen Chen, for his untiring guidance and constant encouragement throughout my candidature. I am indebted to him for his enlightening guidance and generous financial support. I thank Dr. Chen for everything I learned from him.

I would like to thank, My committee member, Dr. Li Cao for giving me valuable suggestion and discussion about Micropump finite element simulation so that I can do finite element simulation smoothly. I also would like to thank Dr. Gray Tuttle for his valuable Microfabrication class and suggestion on my project from the practical point of view. Many thanks also go to Dr. Ranga Narayanaswami for serving in as one of my committee members.

I appreciate Mr.Tony Witt for helping me to use analysis facilities in Microelectronics Research Center in Iowa State University. I would also like to thank Liu Yang to implement numerical simulation code and his inspiration discussion about Computational Fluid Dynamics.

It has been great pleasure to work and interact with my fellow graduate student in Dr. Chen's group. My appreciation goes to my labmates in Microfabrication and Microsystems Laboratory. Senthill P T, Vijay Kancharla, Wei Zheng and Yi Lu.

Last but not the least, I sincerely thank my wife Ms Rong Qian and my parents, whom I owe too much, for their unfailing support throughout my study, without which I cannot further my study in United States.

ABSTRACT

A micropump is one of the most important elements in a micro-total analysis system used for rapid chemical and biological analysis. To date, different kinds of micropumps have been designed, fabricated, tested, and implemented. Among them, a PZT valveless micropump is receiving increasing attentions due to its unique advantages over a conventional check-type micropump. A valveless micropump is short of fatigue and wear of movable part. Without movable parts in the device may avoid high-pressure drop across the valves. It is expected that a valveless micropump has higher reliability and a longer lifetime. In particular, a valveless micropump is unique for delivering solutions with particles.

Diffuser and nozzle elements direction dependent flow characteristics are quantitatively studied and summarized. From diffuser and nozzle flow characteristics, the working principle of the valveless micropump is presented. Based on fluidic mechanics and solid mechanics, a dynamic model for the PZT actuated valveless micropump is developed.

The flow rate and backpressure are the most important performances for the valveless micropump. Considering nonlinear pressure loss in the nozzle, a numerical simulation method is chosen to study the valveless micropump performance. The simulation is studied in low frequency domain. The effects of several key parameters on the micropump performances are discussed. These key parameters include passive plate dimensions, PZT dimensions, and nozzle dimensions. An optimized micropump design is presented following the numerical simulation. The optimized dimensions for the micropump include 500 microns for the membrane thickness, 25 mm for the membrane radius, 80 microns for the nozzle neck and 400 microns for the nozzle length.

The fabrication process for the valveless micropump is also implemented. Two major problems associated with the fabrication process were experimentally investigated. The fabrication process is revised accordingly.

CHAPTER 1

INTRODUCTION

This chapter will provide an overview of Micro Total Analysis System (μ -TAS) including specific components such as different types of microactuators, valves and micropumps. The associated actuation mechanisms are discussed. The valves are of two types: active and passive. Based on these different microactuators and valves, micropumps are also discussed.

1.1 Micro Total Analysis System

Micromachining based on microfabrication of integrated circuits is widely applied to the fabrication of microsensors for measuring physical quantities, such as force, pressure, acceleration, flow and chemical quantities including gas and ion concentration. In the late 1980s, the development of micro actuators by micromachining became popular. A new research area of microelectromechanical systems (MEMS) originated from integrated circuit technique was established. Micro flow control devices, such as micro valves and micro pumps fabricated on a silicon or glass substrate using miniature actuators have been developed. Because of the emphasis on miniaturization of the total chemical analysis, this analysis system is called Micro Total Analysis System (μ TAS). Each element of the chemical analysis system is miniaturized by micromachining and is integrated on a substrate. This process reduces the system size, cost, dead volume, and the amount of reagent needed for measurement. The total process time is also reduced along with a decrease in the power

consumption for the entire system. On the other hand, a detection method realizing highly sensitive measurement with a small sample is required.

The first μ TAS, the micro gas chromatograph (GC) developed by a group from Stanford University in the late 1970s is still commercially available. However, this has not been used widely. In addition to miniaturization of the device and lower price, μ TAS is expected to be applied in areas not previously accessible, such as bedside monitors in clinical use and in onsite environmental analysis. For this purpose, led by researchers in micromachining, research on the elements of μ TAS such as microsensors and micro flow control devices and system realization has been carried out to miniaturize a blood gas concentration analyzer, a flow injection analysis (FIA) system, and high speed liquid chromatographic device.

On the other hand, researchers in analytical chemistry have recognized the importance of micromachining and have carried out research on the fabrication of analytical cells for the preanalysis of samples. In particular, the technique of fabricating capillary electrophoresis cells on a planar substrate has drawn significant attention. Cell miniaturization and reduction of analysis time as well as efficiency enhancement by parallel measurement have been attained. In U. S. and Canada, a national project for analyzing the human genome has been promoted, in which micromachining is used to develop DNA analysis systems.

A conceptual schematic of μ TAS consists of a sample injector (a mechanism for injecting a sample), a pump to control the flow of the carrier and the sample, a mixer/reactor for the reagent, a separator and a sensor. A filter is used in the sample inlet part to prevent plugging of the microchannels. Nowadays, there are two types of integration methods for the entire

micro analytical system: planar configuration and modular configuration. The University of Twente in Netherlands and the Fraunhofer Institute proposed the planar configuration. The planar system consists of a micropump, valves and sensors, and a glass-silicon or plastic substrate with channels connecting the elements. The modular configuration on the other hand has many different function layers. Each function layer performs one analysis step. From the top to the bottom, these different layers are connected with channels. But most of the analytical systems are planar configuration because of its simple and easy integration.

Micropumps and valves are the key components in the analytical system because they pump and control sample flow in the entire system. Therefore it is necessary to pay more attention to the micro pump and valve in order to get a high performance micropump and valve.

1.2 Micropump and Valve

Since 1990s, the attention to micropumps and valves has been increasing rapidly. So far, many different types of pumps and valves have been fabricated. A typical micropump includes an actuator and its connected valves. A micropump actuator may have different actuation mechanisms - electromagnetic, piezoelectric, pneumatic, shape memory alloy (SMA), electrostatic, thermopneumatic, and bimetallic etc. An active valve employs the same kind of actuation such as electromagnetic, piezoelectric, pneumatic, shape memory alloy (SMA), electrostatic, thermopneumatic. A passive valve is also called a check valve, which is one of the most popular valves in micropump design.

1.2.1 Microactuator

The performance of an active valve and a micropump depends strongly on the features of the actuator. In fact, the size of the device is determined by the actuator. Many kinds of actuators have been studied and used.

Electromagnetic actuator is realized with a solenoid plunger. A force developed by these actuators depends on the applied current and on the number of turns. A large stroke can be obtained. Miniaturization is, however, difficult because of the restriction imposed by the size of the solenoid coil.

Piezoelectric actuators using the piezoelectric effect have been widely used. Piezoelectric actuators of disk type, cantilever type and stack type have been commercialized. Simple plate type piezoelectric actuators can be classified into two types - monomorph and bimorph. These actuators consist of piezoelectric ceramic plates and electrodes. Disk type actuators can be easily glued with epoxy resin. These actuators have relatively large deformation and fast response, but the pressure generated is small. To obtain large pressure, stack type structure of many piezoelectric plates and driving electrodes were employed. However, the stroke is often small. This type of actuator can be mounted in a glass tube and bonded to the structure with epoxy resin.

Pneumatic actuator consists of an electromagnetic valve, a leak valve and an air compressor. The displacement and generated force can be widely controlled. In this case, the response time depends mainly on the flow conductance of the valves. But the size reduction is very difficult.

Shape memory alloy (SMA) actuator consists of a shape memory alloy coil to memorize the expanded state and a bias spring. The SMA coil regains its original shape when it is heated above the critical temperature. The bias spring can bias the plate at some place when SMA cools down. It is easy to miniaturize the actuator size but it is difficult to control the displacement precisely.

Electrostatic actuator has a movable electrode and a fixed electrode. The principle of the electrostatic actuators is very simple. When a voltage is applied on the electrodes, an electrostatic force will be generated between the electrodes. This force is inversely proportional to the second power of the distance separating the two electrodes. Hence the available stroke is limited when a reasonable pressure is required.

Thermopneumatic actuator has a sealed pressure chamber and a movable diaphragm. In a typical actuator, the inner gas of the chamber is heated by electrical dissipation in heater resistors incorporated in the chamber. The rising time of the actuator depends on the heat capacitance and the available power of the heater, while the relaxation time is determined by the heat transfer to the external world.

Electromagnetic actuator consists of a soft magnetic mass suspended by a spring beam and an external solenoid coil. The electromagnetically generated pressure is decided by its surface area, the magnetization of the mass, and the vertical component of the magnetic field produced by the external coil. But miniaturization of the external coil is a problem in this case.

Bimetallic actuator consists of a center boss, a circular diaphragm made of bimetallic materials, and a circular heater. By varying the electrical power of the heater and thus the temperature of the bimetal, the displacement of the center boss can be controlled. The generated pressure is proportional to the difference between the thermal expansion coefficients of the two materials and to the temperature difference. Strong force and reasonable displacement can be expected by using an appropriated combination of the two materials. The relaxation time is also the dominant factor in the response time.

The features of all kinds of actuators are summarized in Table 1.1.

Table 1.1 Features of the miniaturized conventional Microactuators

Actuators	Pressure	Stroke	Response time	Reliability
Solenoid plunger	Small	Large	Medium	Good
Disk Piezo	Small	Medium	Fast	Good
Stack Piezo	very large	Very small	Fast	Good
Pneumatic	Large	Large	Slow	Good
SMA	Large	Large	Slow	Good
Electrostatic	Small	Very small	Very fast	very good
Thermopneumatic	Large	Medium	Medium	Good
Electromagnetic	Small	Large	Fast	Good
Bimetallic	Large	Small	Medium	Enough

1.2.2 Micro valve

Micro valves can be classified into two categories: active micro valve (with an actuator) and passive micro valve (without an actuator)

1.2.2.1 Active micro valve

Solenoid plunger micro valve is the first reported micro valve. It consists of a silicon valve seat and a nickel diaphragm actuated by an external solenoid.

Piezoelectric micro valve has a stack type actuator or piezo disk type actuator. This kind of micro valve has a large stroke and very small dead volume. To have disposable flow channel, the channel was separated from the actuator part. Since the actuator part can be reused many times, it reduces the cost and is useful for medical applications. This kind of microvalve is usually used as a normally-closed microvalve.

Shape memory alloy and bias spring micro valve is often used for normally open and closed microvalves. A thin silicon membrane was used as a soft sheet that covers the hole in the flow channel. Large actuator stroke realizes a large flow conductance suitable for liquid flow control. However, this kind of valve can be used only as an on-off valve because of the poor controllability of the SMA actuator.

Electrostatically actuated microvalves have been developed for some time. Simple cantilever type microvalve can be fabricated using surface micromachining, but the generated force of this valve is small when the electrode gap is large. The controllable pressure range is also limited. In order to generate enough force to actuate the valve, the pressure of the fluid can be

used as a balancing force on the moving parts of the valve. The fluid pressure produces an upward direction force to open it. The required force to actuate the valve is only a small fraction of the total pressure of the fluid if the valve is properly designed. This type of valve is made of stacked silicon structure bonded by fusion bonding technique.

A thermopneumatically driven microvalve normally uses a sealed pressure cavity filled with a liquid. A resistive heater was formed on the glass substrate. The chamber can also be heated optically through the glass. Using the liquid-gas phase system of methyl chloride, the pressure can be increased by 0.7 kgf/cm^2 within 5 ms by applying 200 mV. The dynamic range of this valve can be broadened by adjusting the cavity shape, boiling point of the control liquid, and the quantity of both gas and liquid molecules.

A bimetallic beam that provides significant force and displacement was also used for the microvalve. It consists of a diaphragm with a central boss and a bimetallic actuator. The actuator is a circular silicon diaphragm having diffused resistors and an annular aluminum region, which are the elements of the bimetallic structure. The temperature of the bimetallic structure on the diaphragm boss so as to control the gas flow. This valve can control the gas flow ranged from 0 to 90ml/min with an input pressure of 2.1 kgf/cm^2 with no obvious pressure drop. The leakage flow at 1.4 kgf/cm^2 input pressure was about 45ul/min, which corresponds an on-off ratio of about 1600.

An electromagnetically driven microvalve consists of a valve cap and a magnetic coil. The valve cap is made of a Ni-Fe alloy, a soft magnetic material supported by a spring. It moves

vertically in the magnetic field applied by an external electromagnet. The valve was driven by a 0.1 HZ to 100 HZ rectangular magnetic field.

1.2.2.2 Passive microvalve

Microvalves without actuators are mainly used for check valves in a micropump. In a micropump, very small leakage under reversely applied pressure and large reverse to forward flow resistance ratio are required. The response time which means transition time during open-to-close or close-to-open is also an important parameter of the valve. Structures of check valves developed so far are shown in Figure 1.1. It consists of ring mesa structure having a through hole at the center and a surrounding ring diaphragm. Figure 1.1b has a simple cantilever beam structure. Figure 1.1c was fabricated by surface micromachining. A round polysilicon sheet is suspended by four thin polysilicon beams that are fixed on the silicon substrate. Figure 1.1d consists of a thinned V groove with a thin slit. It resembles the valve of a human heart. The valve consists of a perforated thin membrane of polyamide stretched over an opening in the titanium membrane as illustrated in Figure 1.1e. Figure 1.1f has a silicon rubber float and a through-hole. It was made by molding so as to fit precisely into the hole. The float is suspended by four polymer arms fixed to the silicon substrate. Valves of type a, b, c and d have been already used for micropumps. Type f has a very small leakage and large reverse to forward flow resistance ratio at applied pressures larger than 10 mH₂O. This is useful for a very high output pressure micropump.

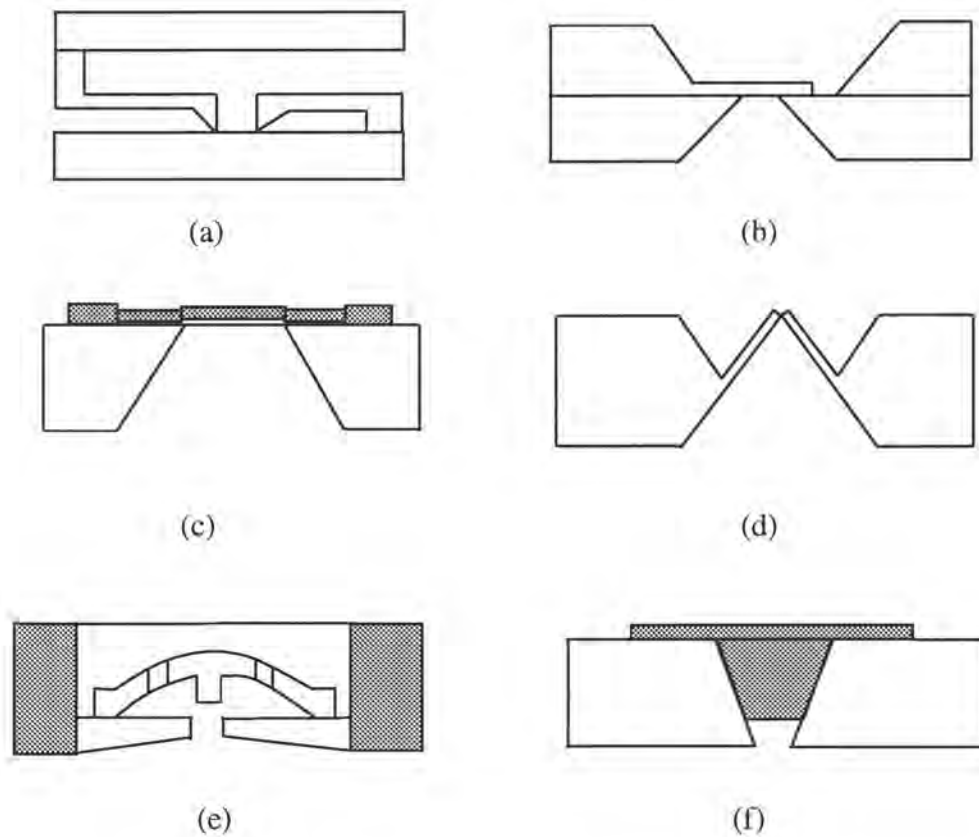


Figure 1.1 Schematics of the passive Microvalve

1.2.3. Micropump

Micro pumps are classified into two groups: mechanical and non-mechanical (without moving parts) pumps. Two kinds of mechanical micropumps have been developed: reciprocating and peristaltic. Many micropumps using different actuators have been fabricated in each type by

micromachining. Electrohydrodynamic effect, electroosmotic phenomena, and ultrasonic effect are used in non-mechanical micropumps.

1.2.3.1 Reciprocating type micropump

This type of micropump consists of a pressure chamber having flexible diaphragm driven by an actuator and passive microvalves (check valves). The check valve and the actuator play very important roles in the flow rate and the maximum output pressure. Many actuators like piezoelectric, pneumatic, electrostatic, thermopneumatic have been used. The maximum output pressure of the micropump depends on the available force of the actuators used.

Piezoelectric disk micropump was the first developed. This type of micropump has been applied for actual system like microflow systems and chemical analyzing systems because of its simple structure and easy assembling.

A piezoelectric micropump uses nozzle/diffuser elements instead of check valves. One of the disadvantages of micropump using the check valves is the restriction of the driving frequency. This type of micropump can be driven at frequency of hundreds of Hz. A water flow rate of about 3.3 ml/min and pump pressure of about 1.0 mH₂O were obtained under driving frequency of 307 Hz and applied voltage of 141 V. the maximum pressure of this pump was 2.5 mH₂O. Another remarkable advantage was the capability of pumping gas. 35 ml/min air pumping was demonstrated under a driving frequency of 6 kHz and a voltage of 20V. This allows one to pump liquid with solid particle content.

A piezoelectric stack micropump uses PZT stack actuator. The actuator offers a large force and high frequency response, a high flow rate up to 100 $\mu\text{L}/\text{min}$ and a maximum pressure of 1.5 mH_2O . Rippleless pumping was carried out by parallel connection of two micropump driven by opposite phase voltage as well as by series connection of a variable pressure chamber that is driven by a piezoelectric stack.

An external pneumatically driven micropump was fabricated using a LIGA process. The micropump is made of a gold structure with a titanium diaphragm. The check valve consists of a titanium membrane and a polyimide membrane. A maximum flow rate of 80 $\mu\text{L}/\text{min}$ and a maximum pressure of 0.47 mH_2O were obtained for air pumping at a driving frequency of 5 Hz.

An electrostatically driven micropump normally consists of four stacked silicon wafers. The check valve is a bulk cantilever formed on the two lower wafers. This can be fabricated fully in a batch process. The driving frequency range is from 1 to 1000 Hz. At a frequency of 400 Hz, a flow rate of 350 $\mu\text{L}/\text{min}$ and a maximum pressure of 2.4 mH_2O were obtained.

A thermopneumatic micropump was fabricated using resistive micro heater. Bulk type check valves were used. The pumping rate was in the range of 0 to 50 $\mu\text{L}/\text{min}$ at a driving frequency of about 5 Hz.

1.2.3.2 Peristaltic type micropump

The other principle of mechanical micropump is the peristaltic drive. Two types of peristaltic micropump were reported using piezo disk and thermopneumatic actuators.

The piezoelectric dimorph type peristaltic micropump has several active valves and pumping is carried out when these valves are driven by controlled signals to achieve peristaltic motion. The pumping rate was around 100 $\mu\text{l}/\text{min}$ when the driving voltage was 80 V. A negative voltage was used to bend the valve down during their closed period. The maximum pressure was 0.6 mH_2O . The flow rate was proportional to the frequency up to 15 Hz.

The thermopneumatically driven peristaltic micropump has several active pressure chambers with flexible membrane. In this case a micro resistive heater was used to change the temperature of the pressure chamber. To heat up the inner gas in the chamber, laser light was used. The flow range is around 90 $\mu\text{l}/\text{min}$. The maximum output pressure is 0.03 mH_2O .

The electrohydrodynamic actuation micropump is limited to fluids of low conductivity and dielectric liquid such as organic solution. Two types of electrohydrodynamic micropumps were presented: a powerful DC charge injection pump and a travelling wave drive pump.

Besides these mechanical micropumps, there are some original non-mechanical micropumps: Electroosmosis micropump and travelling flexural wave (ultrasonic) micropump. Electroosmosis micropump uses electrokinetic phenomena of electroosmosis. A traveling flexural wave (ultrasonic) micropump uses traveling flexural wave for transportation of liquids. Liquids can move in the directions of wave propagation with speeds proportional to the square of the acoustic amplitude. Both micropumps are not common in the microfluidics.

Table 1.2 Summary of Micropump Performances

Type	Actuator	Valve	Flow Range	Max Output Pressure	Driving frequency
Reciprocating	Piezo Disk		8 ul/min	1.0 mH ₂ O	3Hz
		Valveless	3.3 ml/min	2.4 mH ₂ O	
	Piezo Stack		40 ul/min	1.5 mH ₂ O	40Hz
	Pneumatic		80 ul/min	0.47 mH ₂ O	
	Electrostatic		350 ul/min	2.4 mH ₂ O	1000Hz
	Thermo-Pneumatic		58 ul/min	0.3 mH ₂ O	5Hz
Peristaltic	Piezo disk		100ul/min	0.6 mH ₂ O	15Hz
	Thermo-Pneumatic		90ul/min	0.03 mH ₂ O	3Hz

1.3 Valveless Micropump

In microfluidics, a valveless micropump is paid more and more attention due to many advantages compared to a check micropump. Because of the absence valves, the micropump is short of fatigue and wear of movable parts. Moreover, pumps without movable valves may avoid high-pressure drop across the valves. Therefore, a valveless micropump has higher reliability and longer lifetime. In particular for microanalysis systems, the solution may have

tiny particle inside. These particles may block the channels of the analysis system or damage the check valves, so it is advantageous to use a valveless micropump for microanalysis system.

The first valveless micropump was reported in 1992 by Ritcher et al. The successful employment of diffusers as passive valves was first demonstrated by Stemme and Stemme (1993). The first successful nozzle micropump was fabrication by Torsten Gerlach in 1995. However, the performances of these micropumps are not good enough for microsystem analysis. The backpressure of the first diffuser micropump was 2 mH₂O, but the bump is fairly big and is difficult to be fabricated using MEMS technology. The backpressure of the first diffuser micropump was only 4 kPa. This is far from what is needed.

At the same time, a lot of researchers studied diffuser and nozzle direction dependent flow characteristics. Anders Olsson et al numerically and experimentally studied diffuser flow characteristics in 1997 and 2000, Torsten Gerlach analyzed the nozzle flow in 1997, and M. Heschel et al experimentally study the nozzle and diffuser flow performances in 1997. In order to improve valveless micropump performances, dual chamber method was proposed (Amos Ullman 1998). Based on this idea, the first parallel dual chamber diffuser micropump was demonstrated (Anders Olsson et al 1996). And a micromachined flat-walled valveless diffuser pump was successfully fabricated (Anders Olsson et al 1997) a year later. This micromachined flat-walled dual chamber diffuser pump significantly improved the micropump performance. A maximum backpressure of about 7mH₂O and a maximum flow rate is 2.3 ml/min was obtained. Though the first nozzle micropump was fabricated in 1995,

the performances of nozzle micropump has not been improved. Compared to diffuser micropump, nozzle micropump is easier to fabricate with MEMS technology and to integrate with a microanalysis system.

Several models have been developed to study a diffuser micropump and nozzle micropump (Anders Olsson et al 1999, Fred Forster et al 1996 and Torsten Gerlach et al 1995). For the diffuser micropump, one dynamic model was reported in 1999 (Anders Olsson et al). But this dynamic model is rather complicated for a diffuser micropump. For the nozzle micropump, only static models were available. But the micropump has to practically work in dynamic conditions.

Although a lot of work has been done for valveless micropumps. Little work has been carried out to improve the performance of nozzle micropump for micro-analytical systems and it is necessary to develop a dynamic model to study the nozzle micropump.

1.4 Thesis Organization

This thesis is aimed at building a dynamic model to investigate effects of the micropump design parameters on micropump performances such as flowrate and backpressure. Based on the investigation, an optimized nozzle micropump design is achieved. A reliable fabrication process is also presented.

In Chapter 2, the direction dependent flow characteristics of the diffuser and nozzle elements are quantitatively studied and summarized. From diffuser and nozzle flow characteristics, the

working principle of a valveless micropump is presented. Based on fluid flow theory and solid plate and shell theory, a dynamic PZT valveless micropump model is developed.

Chapter 3 deals with the numerical simulation. The flowrate and backpressure are chosen as the studied performances for a valveless micropump. Due to the nozzle nonlinear pressure loss, numerical simulation method is chosen to study the valveless micropump. Based on numerical simulation, the effects of several key parameters on valveless micropump performances are discussed. These key parameters include passive plate dimensions, PZT dimensions, and nozzle dimensions. From the results, an optimized micropump design is achieved. This optimized micropump dimensions are 500 microns for membrane thickness, 25000 microns of membrane radius, 80 microns of nozzle neck, and 400 microns for nozzle length. All simulation is implemented in a low frequency domain.

In Chapter 4, a reliable fabrication process is developed based on experimental verification. At the same time, two major fabrication problems are analyzed and alternative solutions are also proposed.

Chapter 5 summarizes the conclusions of present study and suggests direction for future research about a valveless micropump.

CHAPTER 2

MODELING OF PZT VALVELESS MICROPUMP

In this chapter, diffuser and nozzle element direction dependent flow characteristics are discussed. Based on this discussion, the principle of the valveless micropump is addressed. From the mass conservation theory and extend Bernoulli equation, a dynamic micropump model is developed.

2.1 Principle of Valveless Micropump

Valveless micropump uses two kinds of passive valves: diffuser and nozzle. Based on diffuser valve or nozzle valve, valveless micropump can be categorized into a diffuser valveless micropump and a nozzle valveless micropump.

2.1.1 Diffuser Element Analysis

The diffuser element is the part of the valveless diffuser pump that provides the pump its flow direction properties. The actual diffuser uses the part with diverging cross section in the positive direction. A diffuser is by definition a device for reducing the velocity and increasing the static pressure of a fluid passing through a system. It is often used in internal flow systems. The reduction of the velocity for an expanding cross section follows from the continuity equation. The static pressure is therefore increased according to Bernoulli's equation. The geometry of the diffuser is very simple, but the flow in it is very complex. Due

to the negative pressure gradient the flow may separate from the sidewall which causes large pressure losses that deteriorates the function of the diffuser. For micromachined diffusers, the reported data is limited. It is important to give an explanation of the working principle of the diffuser element and estimate the diffuser element efficiency based on empirical results in the literature.

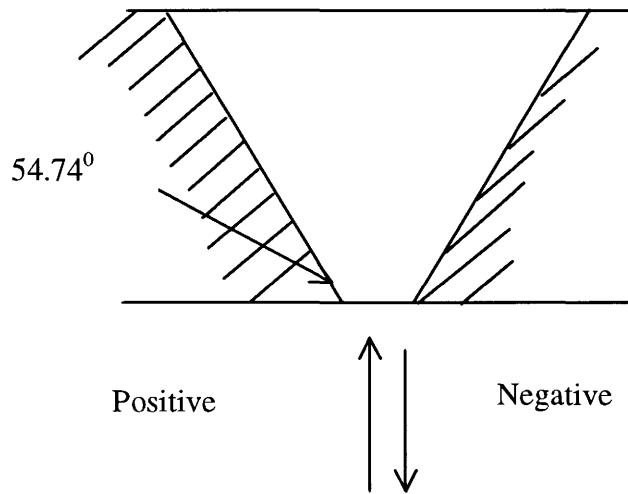


Figure 2.1 Diffuser Element Section View

The pressure loss in internal flow systems is normally given by a loss coefficient K that is related with the pressure drop Δp by

$$\Delta p = K \rho u^2 / 2, \quad (2.1)$$

where ρ is the fluid density and u is the mean velocity in the upstream.

For a diffuser element, it is practical to relate the pressure loss to the narrowest cross section, the neck by

$$\Delta p = \xi \rho u_{neck}^2 / 2, \quad (2.2)$$

where ξ is the pressure loss coefficient and u_{neck} is the mean velocity in the neck. The relation between K and ξ is simple geometrical area relation given by

$$\xi = KA \left(A_{neck} / A_{upstream} \right)^2 \quad (2.3)$$

If interactions between the different parts of the diffuser element are neglected, the total pressure loss can be calculated as the sum of the losses on the different parts.

In order to achieve the best pump performance the losses in the positive direction should be minimized while maximizing the losses in the negative direction. At the outlet, the flow always forms a jet regardless of the shape and $K=1$. At the inlet, the losses should be small in the positive direction. This is achieved with a rounded inlet and $K=0.05$. In the negative direction the losses should be as high as possible and a sharp inlet is used with $K=1$.

Experimental data for diffusers are commonly presented as performance maps in literature [David Japikse et al 1998]. From such a performance map, the maximum pressure recovery C_p for the diffuser can be estimated and the loss coefficient can be calculated as

$$K_{diffuser} = 1 - \left(A_{in} / A_{out} \right)^2 - C_p, \quad (2.4)$$

where A_{in} is the inlet area and A_{out} is the outlet area. The losses are minimized when C_p is maximized. From the diagram performance map in literature [David Japikse et al 1998], we

find that $C_p = 0.77$. It is known that the performance is highly dependent on the boundary conditions at the inlet. In the opposite direction the losses are always small, with K approximately 0.03.

The pressure loss coefficients for the different regions are summarized in Table 2.1 with the diffuser efficiency ratios η calculated as

$$\eta = \zeta_{negative} / \zeta_{positive} \quad (2.5)$$

In the high frequency domain, the mass inertia of any fluid counteracts acceleration $\partial Q / \partial t$ resulting in a pressure drop. This phenomenon can be described by the hydraulic inductivity L . The inductivity of a flow path section of length S and cross section A is defined as

$$L = \rho \frac{S}{A} \quad (2.6)$$

For equally distributed velocity over cross section, the inductivity of the fluid inside the diffuser can be calculated by

$$\begin{aligned} L &= \rho \int_0^s \frac{1}{A(z)} dz = \frac{\rho}{A_0} \int_0^s \frac{1}{[1 + 2 \frac{z}{d} \tan(\frac{\alpha}{2})]^2} dz \\ &= \frac{\rho}{A_0} \int_0^s \frac{1}{[1 + 2\xi \tan(\frac{\alpha}{2})]^2} d\xi \end{aligned} \quad (2.7)$$

Assuming that the minimum diffuser and nozzle element length is the place that 90% kinetic energy is converted into pressure, we have

$$S_{min} = \frac{1}{2 \tan(\frac{\alpha}{2})} \frac{1}{\sqrt[4]{1-0.99}} - 1 \quad (2.8)$$

The minimum inductivity is obtained as

$$L_{0,\min} = \frac{\rho}{A_0} \int_0^{s_{\min}} \frac{1}{[1 + 2\xi \tan(\frac{\alpha}{2})]^2} d\xi = 0.342 \frac{\rho d}{A_0} \frac{\cos \alpha}{1 - \sin \alpha} \quad (2.9)$$

The maximum inductivity is calculated as

$$L_{0,\max} = \frac{\rho}{A_0} \int_0^{\infty} \frac{1}{[1 + 2\xi \tan(\frac{\alpha}{2})]^2} d\xi = \frac{1}{2} \frac{\rho d}{A_0} \frac{\cos \alpha}{1 - \sin \alpha} = 1.46 L_{0,\min} \quad (2.10)$$

Because of the divergence of diffuser, the velocity will be smaller and smaller during flow inside a channel, whereas, the velocity of diffuser will be bigger and bigger owing to convergence.

From the above discussion, we have

$$L_{0,\text{negative}} > L_{0,\text{positive}} \quad (2.11)$$

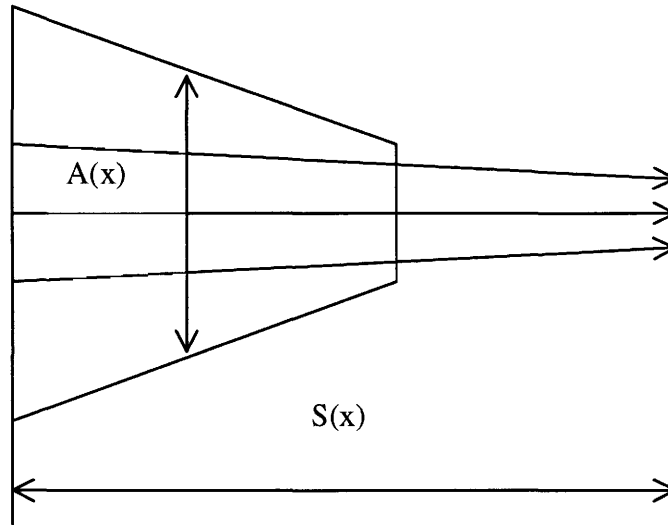


Figure 2.2 Diffuser flow in the positive direction

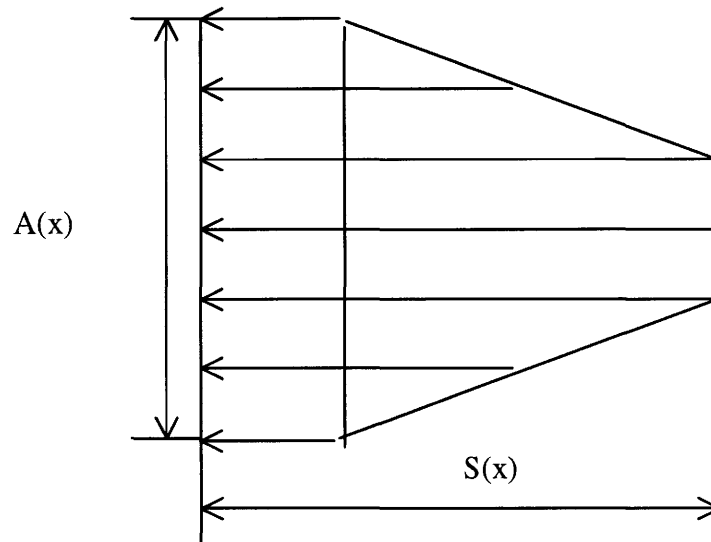


Figure 2.3 Diffuser flow in the negative direction

2.1.2 Nozzle Element Analysis

The same type of analysis can be made for a nozzle element in the dynamic micropump, henceforth called valveless nozzle pump. A nozzle element is a flow channel with a large opening in the positive direction as illustrated in Figure 2.4.

The nozzle elements depend on a different mechanism when compared to diffuser elements. The nozzle element depends on the inlet edge at the narrowest part and the “vena-contracta” effect. The diverging angle direction does not work as a diffuser since no pressure is

recovered and the losses are higher than for sudden expansion. The converging wall direction is the positive direction.

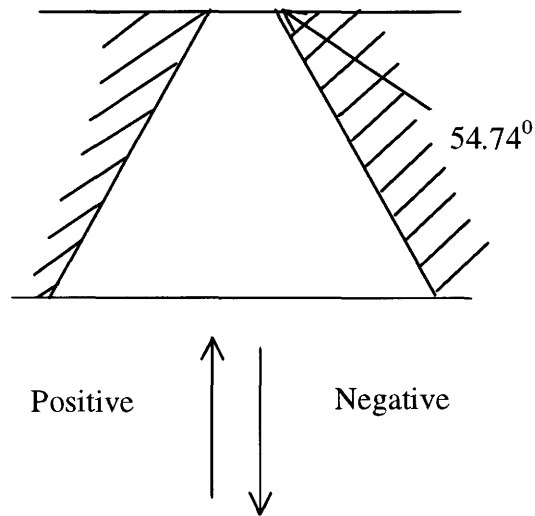
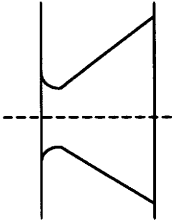
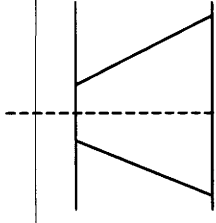
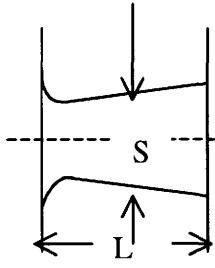
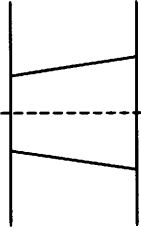


Figure 2.4 Nozzle Element Section View

Since available data is for conical diffusers calculation was done assuming a conical element with dimensions according to Table 2.1 and positive and negative according to Figure 2.2. The resulting pressure loss coefficients and flow inductivity are summarized in Table 2.1

Table 2.1 Summarization of flow efficiency of different nozzle and diffuser elements

	a=70°	a=70°	a=5°	a=5°
				
ξ_+	1.1	1.1	1	1
ξ_-	1.4-1.6	1.05-1.25	0.55-0.7	0.2-0.35
α_+	$\frac{1.1L}{d_0(d_0 + Lctg\alpha)}$	$\frac{1.1L}{d_0(d_0 + Lctg\alpha)}$	$\frac{1.05L}{d_0(d_0 + Lctg\alpha)}$	$\frac{1.05L}{d_0(d_0 + Lctg\alpha)}$
α_-	$\frac{1.05L}{d_0(d_0 + Lctg\alpha)}$	$\frac{1.05L}{d_0(d_0 + Lctg\alpha)}$	$\approx \frac{1.05L}{d_0(d_0 + Lctg\alpha)}$	$\approx \frac{1.05L}{d_0(d_0 + Lctg\alpha)}$

2.2 Principle of Valveless Micropump

The basic valveless micropump consists of two diffuser or nozzle elements connected to a fluid cavity volume with an oscillating diaphragm. Figure 2.5 is a PZT nozzle valveless micropump configuration.

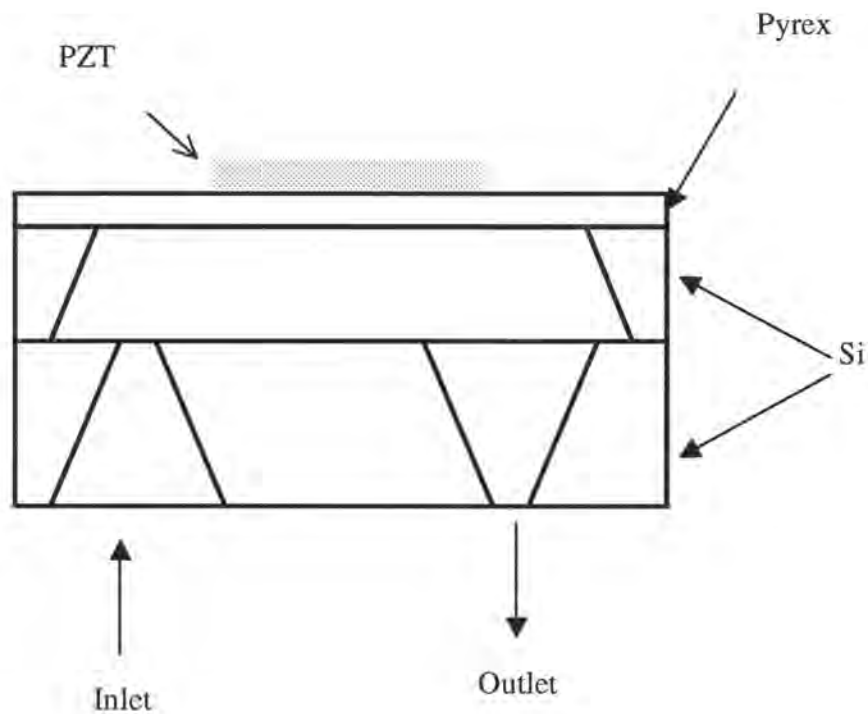


Figure 2.5 PZT Valveless Micropump

A diffuser is an expanding duct and a nozzle is a converging duct. The following-direction action in the valveless micropump is based on the fact that a diffuser or nozzle element can be geometrically designed to have a lower pressure loss in the nozzle direction than in the diffuser direction, for the same flow velocity.

When increasing the chamber volume (the supply mode), the inlet element acts as a nozzle with a lower flow restriction than the outlet element, which acts as a diffuser. This means that a large volume is transported through the inlet chamber than through the output, as shown in Figure 2.6.

When decreasing the chamber volume (the pump mode), the outlet element acts as a nozzle with a lower flow resistance than the inlet element, which acts as a diffuser. This means that a larger volume is transported through the outlet of the chamber than through the input, as shown in Figure 2.7.

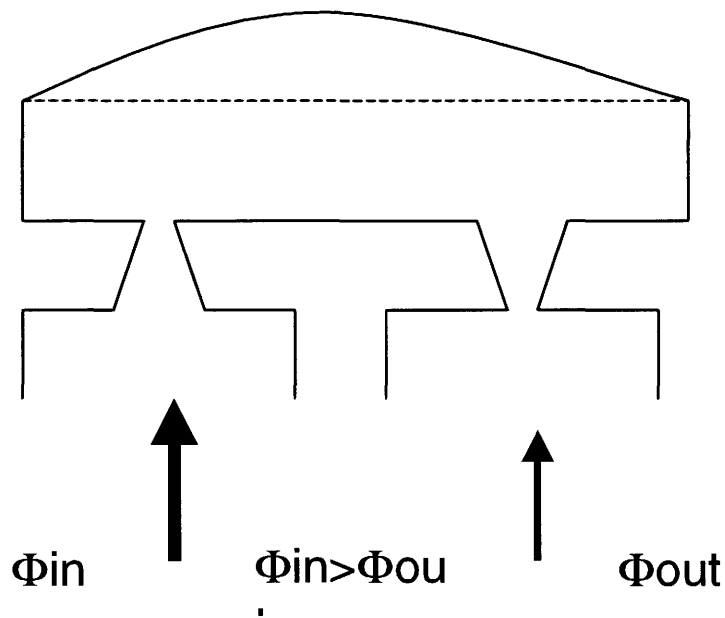


Figure 2.6 Valveless Micropump Supply Working Mode

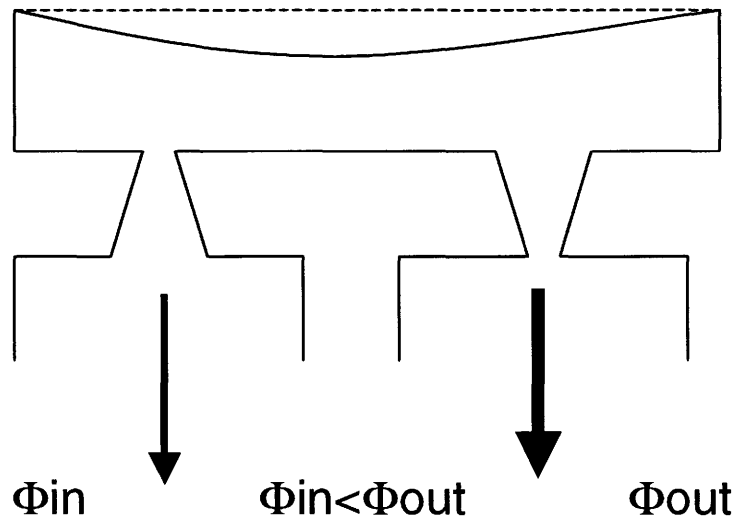


Figure 2.7 Valveless Micropump Pumping Working Mode

The result for a complete pump cycle is therefore that a net volume is transported from the inlet side to the outlet side, despite the fact that the nozzle or diffuser conveys fluid in both directions.

2.3 Modeling of PZT Valveless Micropump

From the above discussion, the principle of the valveless micropump is elucidated. Based on the above discussion and conventional solid mechanics and fluid flow theory, a dynamic model is developed in this work.

2.3.1 Modeling of PZT micropump membrane

Due to small deflection, the system can be thought as a linear system: so the membrane deflection can be divided into two parts, one induced by the PZT electrostatic force and the other induced by fluid pressure inside the chamber. Because the weight of the membrane and PZT mass are far less than fluid pressure force and PZT electrostatic force, it is reasonable to omit the membrane and PZT inertial force. Therefore, the problem is simplified into quasistatic problem.

$$V_{dia} = V_{dia}(U, t) + V_{dia}(P(t)) \quad (2-12)$$

For PZT electrostatic force

$$E_3 = -\frac{U}{H_f} \quad (2-13)$$

The strains in the three directions are

$$\varepsilon_x = d_{31}E_3 \quad (2-14)$$

$$\varepsilon_y = d_{31}E_3 \quad (2-15)$$

$$\varepsilon_z = d_{33}E_3 \quad (2-16)$$

The stress are induced by the electrical field as

$$\sigma_x = C_{13}\varepsilon_z - e_{31}E_3 \quad (2-17)$$

$$\sigma_y = C_{13}\varepsilon_z - e_{13}E_3 \quad (2-18)$$

$$0 = C_{33}\varepsilon_z - e_{33}E_3 \quad (2-19)$$

The solution to the above model is

$$\varepsilon_z = \frac{e_{33}}{C_{33}}E_3 \quad (2-20)$$

$$\sigma_x = \sigma_y = \left[\frac{C_{13}}{C_{33}}e_{33} - e_{31} \right] E_3 \quad (2-21)$$

Since the PZT thin film is stuck to the membrane, the strain will cause in-plane stresses inside the membrane. The in-plane stresses produce a bending moment as

$$M \approx \sigma_x H_f H_d / 2 \quad (2-22)$$

Substituting equation (2-17)

$$M \approx -[\frac{C_{13}}{C_{33}} e_{33} - e_{31}] U H_d / 2 , \quad (2-23)$$

where H_f is the PZT film thickness and H_d is the membrane thickness.

If PZT dimension is close to membrane dimension, it is reasonable to assume that PZT has the same diameter with membrane for simplification. Hereby, we assume the membrane boundary condition is simply support at the first.

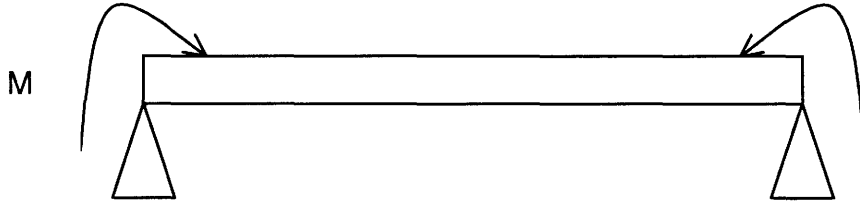


Figure 2.8 Membrane Plate Force View

The displacement of the membrane $W(r)$ caused by moment is given by

$$W_1(r) = \frac{M}{2D(1+\gamma)}(a^2 - r^2) \quad (2-24)$$

Therefore, the volume change induced by PZT is

$$V = \int_0^a W_1(r) dr = \int_0^a \frac{M}{2D(1+\gamma)}(a^2 - r^2) dr = \frac{Ma^3}{D(1+\gamma)} \quad (2-25)$$

For uniform distributed pressure P , the displacement $W(x,y)$ equation from reference [S.Timoshenko et al 1995]

$$\frac{\partial^4 W}{\partial x^4} + 2\frac{\partial^4 W}{\partial x^2 \partial y^2} + \frac{\partial^4 W}{\partial y^4} = \frac{P}{D_0 h^3} \quad (2-26)$$

We assumed that

- a. The diaphragm is fully clamped on its edges
- b. Diaphragm bending is elastic
- c. Deflection $W(x,y,p)$ remains small compared to h

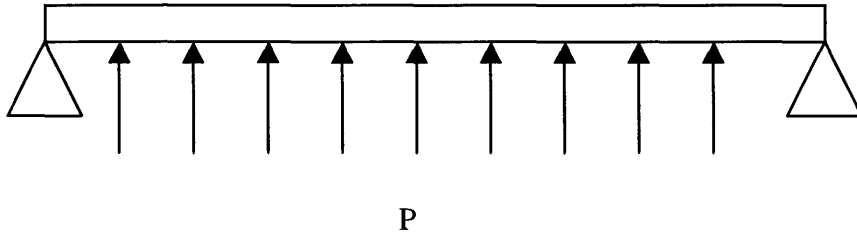


Figure 2.9 Plate deformation under uniform pressure p

For a uniform load P,

$$W_2 = \frac{P(a^2 - r^2)}{64D} \left(\frac{5 + \gamma}{1 + \gamma} a^2 - r^2 \right) \quad (2-27)$$

2.3.2 Conservation of Mass and Coupling of PZT and the Fluid

The conservation of mass from reference [Frank M. White 1991]

$$\frac{d}{dt} \left(\iiint_{cv} \rho \, dv \right) + \iint_{cs} \rho (u \cdot n) \, dA = 0 \quad (2-28)$$

where CV is the control volume, CS is the control surface

Figure 2.6 shows the control volume and control surface. Because of innegligible bubble effect on the micropump performance, a certain volume of bubble is assumed to be entrapped inside the micropump chamber.

After substitution, Equation (2-28) can be changed into

$$\frac{d}{dt} [\rho_{liquid}(p(t)) V_{liquid}(p, t) + \rho_{gas}(p) V_{gas}(p)] - \rho_{liquid} (\Phi_{in} - \Phi_{out}) = 0 \quad (2-29)$$

$$V_{liquid}(p, t) = V_{chamber}(p) + V_{dia}(p, E, t) - V_{gas}(p) \quad (2-30)$$

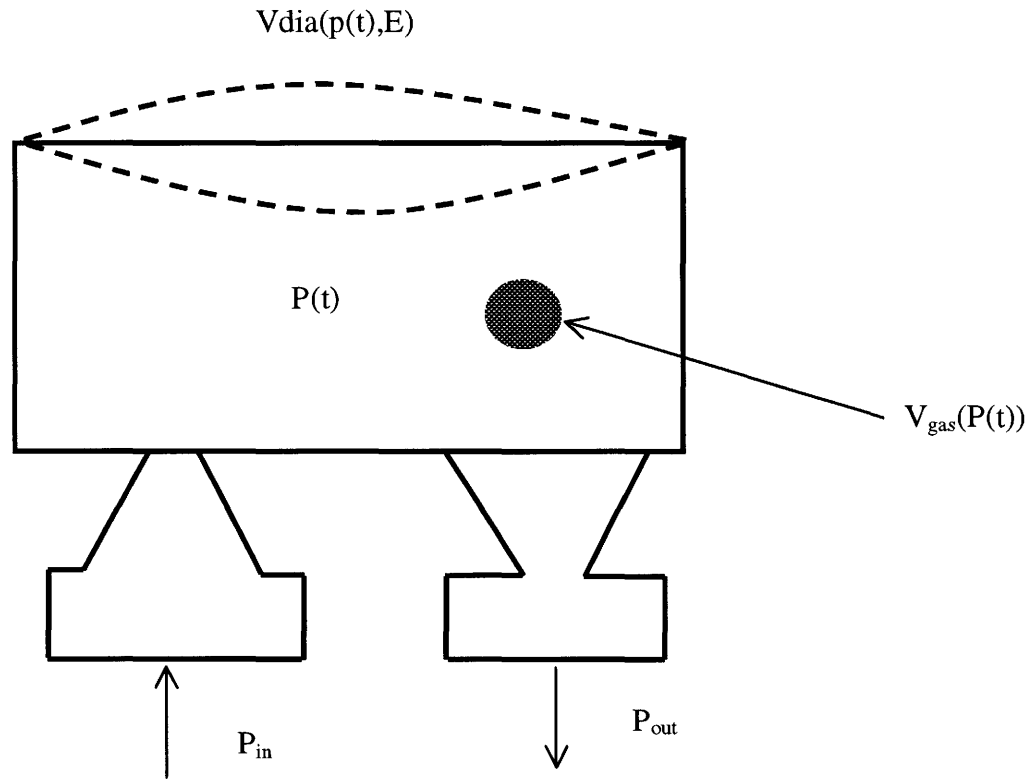


Figure 2.10. Pump Chamber Control Volume

Here we assume 1) incompressible flow 2) except membrane, no chamber volume variation

From (2-29) and (2-30), we have

$$\rho_{liquid} \left(\frac{dV_{dia}}{dp} \frac{dp}{dt} + \frac{dV_{dia}}{dU} \frac{dU}{dt} \right) - \rho_{liquid} \frac{dV_{gas}}{dp} \frac{dp}{dt} + \rho_{gas}(p) \frac{dV_{gas}(p)}{dt} + V_{gas}(p) \frac{d\rho_{gas}(p)}{dt} = \rho_{liquid} (\Phi_{in} - \Phi_{out}) \quad (2-31)$$

Hereby, it is reasonable to assume that the bubble is an ideal gas, which means no heat exchange with the outside micropump chamber. At the same time, the entrapped gas cannot escape to outside. In other words, the mass of gas inside the chamber is conservative.

$$(\rho_{gas}(p) + \Delta\rho)(V_{gas}(p) + \Delta V) = \rho_{gas}(p) V_{gas}(p) \quad (2-32)$$

From Equation (2-32),

$$\frac{dp}{dp} = - \frac{\rho_{gas}(p)}{V_{gas}(p)} \frac{dV}{dp} \quad (2-33)$$

For an ideal gas, the following equation can be obtained

$$\frac{dV_{gas}}{dp} = - \frac{V_{gas,0} P_0}{(P + P_0)^2} \quad (2-34)$$

where P_0 is the atmosphere pressure, V_{gas0} is the gas volume at atmosphere pressure, P is the pressure inside chamber

After substitution (2-34), equation (2-31) is changed into

$$\rho_{liquid} \left(\frac{dV_{dia}}{dp} \frac{dp}{dt} + \frac{dV_{dia}}{dU} \frac{dU}{dt} \right) - \rho_{liquid} \frac{dV_{gas}}{dp} \frac{dp}{dt} = \rho_{liquid} (\Phi_{in} - \Phi_{out}) \quad (2-35)$$

Canceling liquid density,

$$\frac{dV_{dia}}{dp} \frac{dp}{dt} + \frac{dV_{dia}}{dU} \frac{dU}{dt} - \frac{dV_{gas}}{dp} \frac{dp}{dt} = \Phi_{in} - \Phi_{out} \quad (2-36)$$

Substitution (2-34)

$$\frac{dV_{dia}}{dp} \frac{dp}{dt} + \frac{dV_{dia}}{dU} \frac{dU}{dt} + \frac{V_{gas,0} P_0}{(P + P_0)^2} \frac{dp}{dt} = \Phi_{in} - \Phi_{out} \quad (2-37)$$

2.2.3 Dynamic Equation about Nozzle (Extended Bernoulli Equation)

For micropump design, the inlet and outlet are chose as nozzle. According to practical consideration, the following assumptions were made

- 1) Incompressible flow
- 2) Steady flow
- 3) Flow along a streamline

For one dimension flow, extended Bernoulli equation is given by

$$gz_{in} + \frac{P_{in}}{\rho} + \frac{1}{2} \psi_{in} \overline{U_{in}}^2 = gz_{out} + \frac{P_{out}}{\rho} + \frac{1}{2} \psi_{out} \overline{U_{out}}^2 + L \frac{d\Phi}{dt} + \frac{\Delta P_{loss}}{\rho} \quad (2-38)$$

For constant velocity over the cross-section and the same cross-section area and velocity profile at inlet and outlet neck, we have

$$\psi_{in} = \psi_{out} \quad (2-39)$$

So equation (2-38) can be changed into the following

$$gz_{in} + \frac{P_{in}}{\rho} = gz_{out} + \frac{P_{out}}{\rho} + L \frac{d\Phi}{dt} + \frac{\Delta P_{loss}}{\rho} \quad (2-40)$$

For the inlet

$$P_{in} = P(t) + \rho L \frac{d\Phi_{in}}{dt} + \Delta P_{loss} + \rho gH \quad (2-41)$$

For the outlet

$$P_{out} = P(t) - \rho L \frac{d\Phi_{out}}{dt} - \Delta P_{loss} - \rho gH \quad (2-42)$$

To summarize, a dynamic model of passive dynamic valve PZT micropump is achieved. The following three equations describe the dynamic performance of the micropump.

$$\frac{dV_{dia}}{dp} \frac{dp}{dt} + \frac{dV_{dia}}{dU} \frac{dU}{dt} + \frac{V_{gas,0} P_0}{(P + P_0)^2} \frac{dp}{dt} = \Phi_{in} - \Phi_{out} \quad (2-37)$$

$$P_{in} = P(t) + \rho L \frac{d\Phi_{in}}{dt} + \Delta P_{loss} + \rho gH \quad (2-41)$$

$$P_{out} = P(t) - \rho L \frac{d\Phi_{out}}{dt} - \Delta P_{loss} - \rho gH \quad (2-42)$$

CHAPTER 3

SIMULATION OF A VALVELESS MICROPUMP

In this chapter, a numerical simulation algorithm is chosen based on the micropump dynamic model discussed in Chapter 2. A numerical simulation program is developed with Fortran 99. Based on the numerical simulation, the effects of several key parameters such as passive plate dimension, PZT dimension and nozzle dimension on the micropump performance are discussed. The performances of micropump include the flow rate and the backpressure.

3.1 Algorithm of Simulation

In Chapter 2, a set of differential equations defining the micropump were derived. In order to analyze the micropump performance, we must implement some reliable and effective algorithm to solve this set of differential equations. Because of the fact that, pressure loss is nonlinear, a numerical simulation is an effective method to solve this kind of nonlinear problem. Hereby we use a numerical iteration method that is implemented with Fortran 99.

Normally, a micropump works in a low frequency domain. , Therefore, in this work we focus on the micropump performance in the low frequency domain. In the simulation, the working frequency is set to 50 HZ.

The flow rate and backpressure are the most important performances of a micropump. In the following optimization, the relationship between the flow rate and backpressure and some

parameters such as membrane and nozzle dimensions are discussed. Based on the simulation results and fabrication feasibility, the optimized design can be achieved.

3.2.Simulation Results and Discussions

From the micropump schematic in Chapter 2, a PZT actuator is glued on the glass membrane as the actuation source. Because of the PZT actuator vibration, the fluid is sucked in and pushed out of the pump chamber. It is obvious that passive plate membrane has a large influence on the micropump performance. The effect of membrane dimension on the flow rate and the backpressure is discussed in the following section.

3.2.1 Membrane Dimensions Effect on Flowrate and Backpressure

From Figure 3.1 and 3.2, it is observed that the flow rate and backpressure decrease with membrane radius, and vice versa. The micropump chamber volume variation includes variation caused by PZT and the pressure inside the chamber. The volume variation caused by PZT and pressure inside the chamber increase with membrane radius. However, the net volume variation caused by PZT and the pressure inside the chamber decreases with membrane radius. It is not difficult to see why both flow rate and backpressure inversely change with the membrane radius. For the same reason, the net chamber volume variation increases with membrane thickness, so back pressure and flow rate will be bigger with a thicker membrane. The experiment in [Ron L Bardell et al] shows the same result.

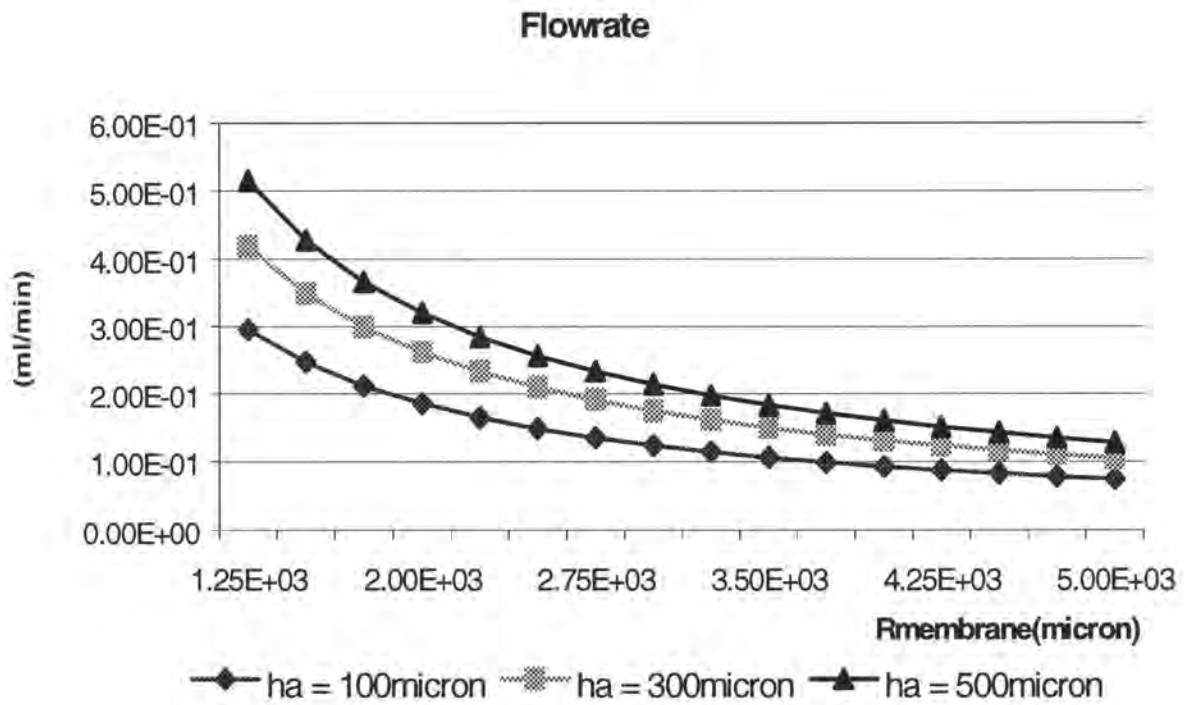


Figure 3.1 Flow rates at different membrane thickness and membrane radius

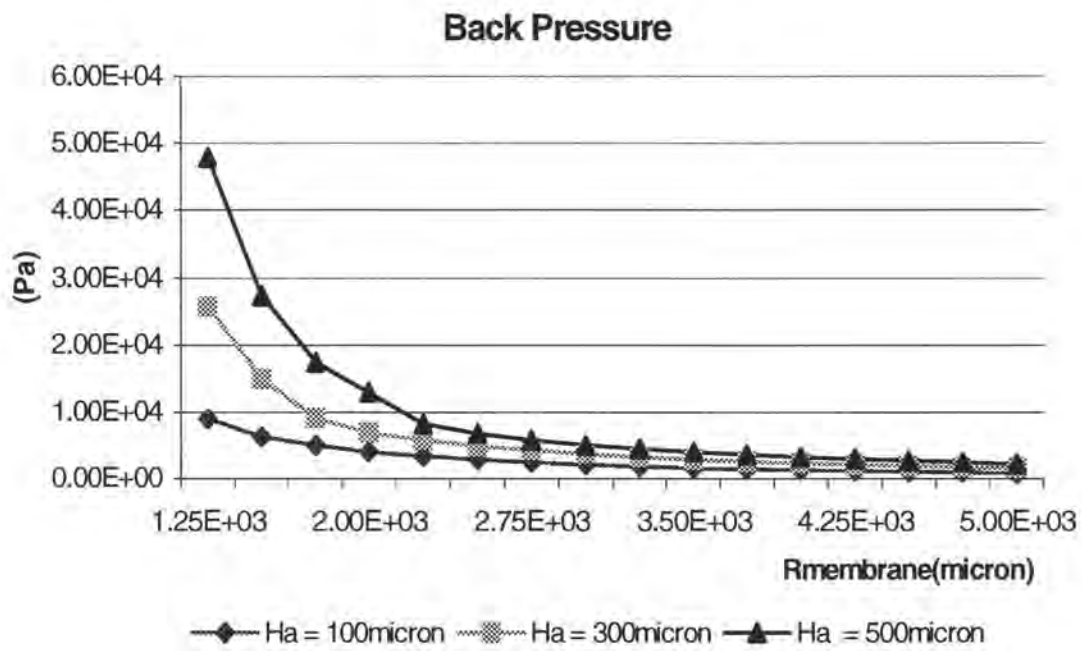


Figure 3.2 Backpressure at different membrane thickness and membrane radius

3.2.2 Nozzle Dimension Effect on Flowrate and Backpressure

The inlet and outlet of the micropump are nozzle elements, so the dimension of the nozzle may have some influence on the performance of the micropump. The relationship between the backpressure and flow rate and the nozzle dimension are discussed in the following section.

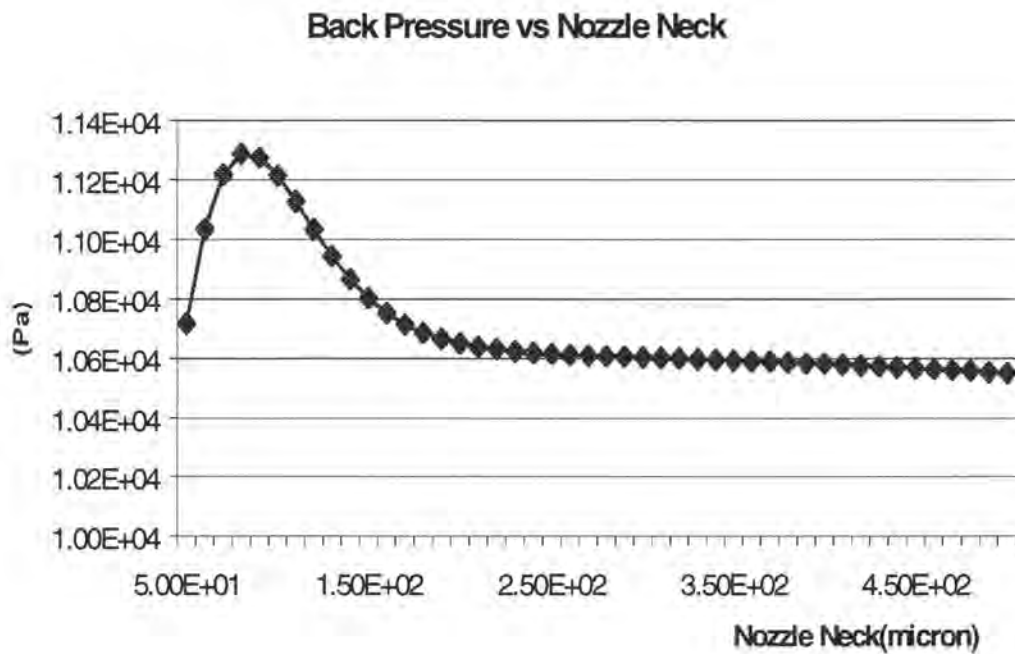


Figure 3.3 Effect of Nozzle Neck dimension on backpressure

From Figure 3.3, we can see the backpressure increases rapidly around the nozzle neck dimension of 80 microns. This coincides with experimental results the micropump has bigger flow rate and backpressure around neck dimension 80 microns (Forster, 1999). From Figure 3.6, it is observed that the nozzle length has little influence on backpressure.

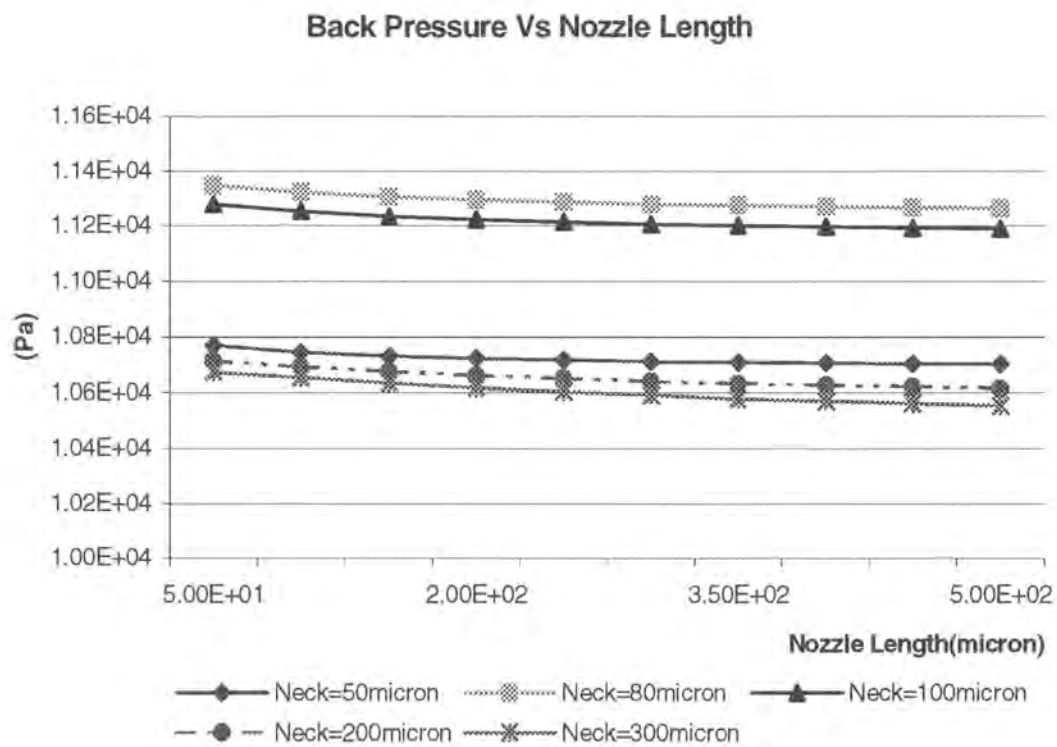


Figure 3.4 Effect of Nozzle Length on Backpressure

Figure 3.5 shows the flow rate increases with nozzle neck dimension. The relationship is nearly quadratic. But, from Figure 3.6, the flow rate does not have any significant change with increase in nozzle length.

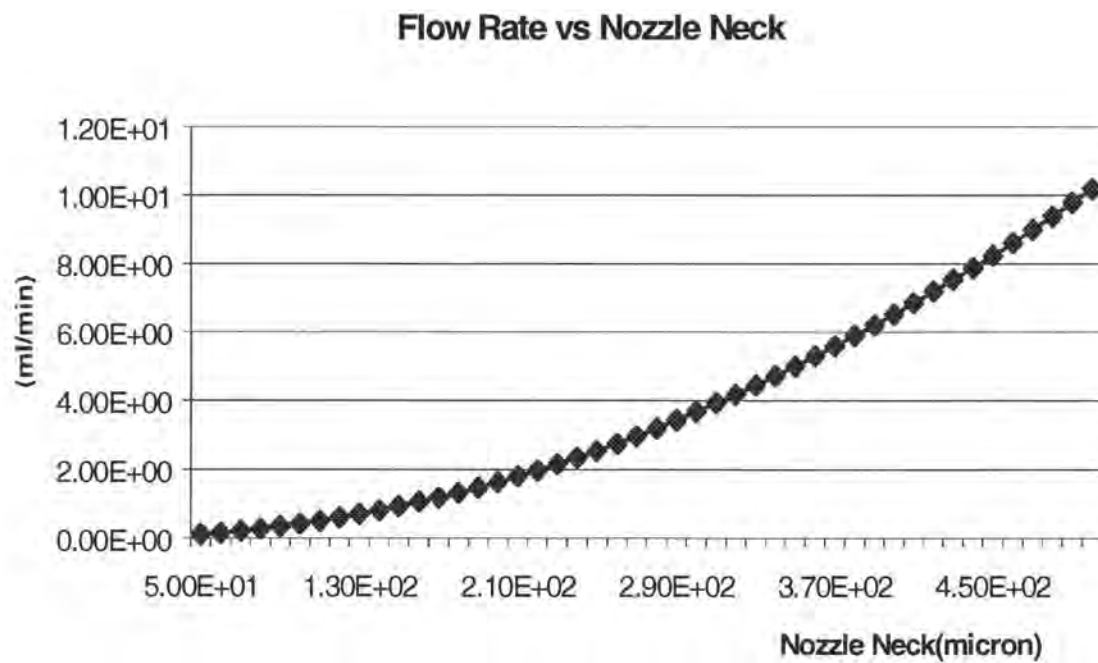


Figure 3.5 Effect of Nozzle Neck Dimension on Flow Rate

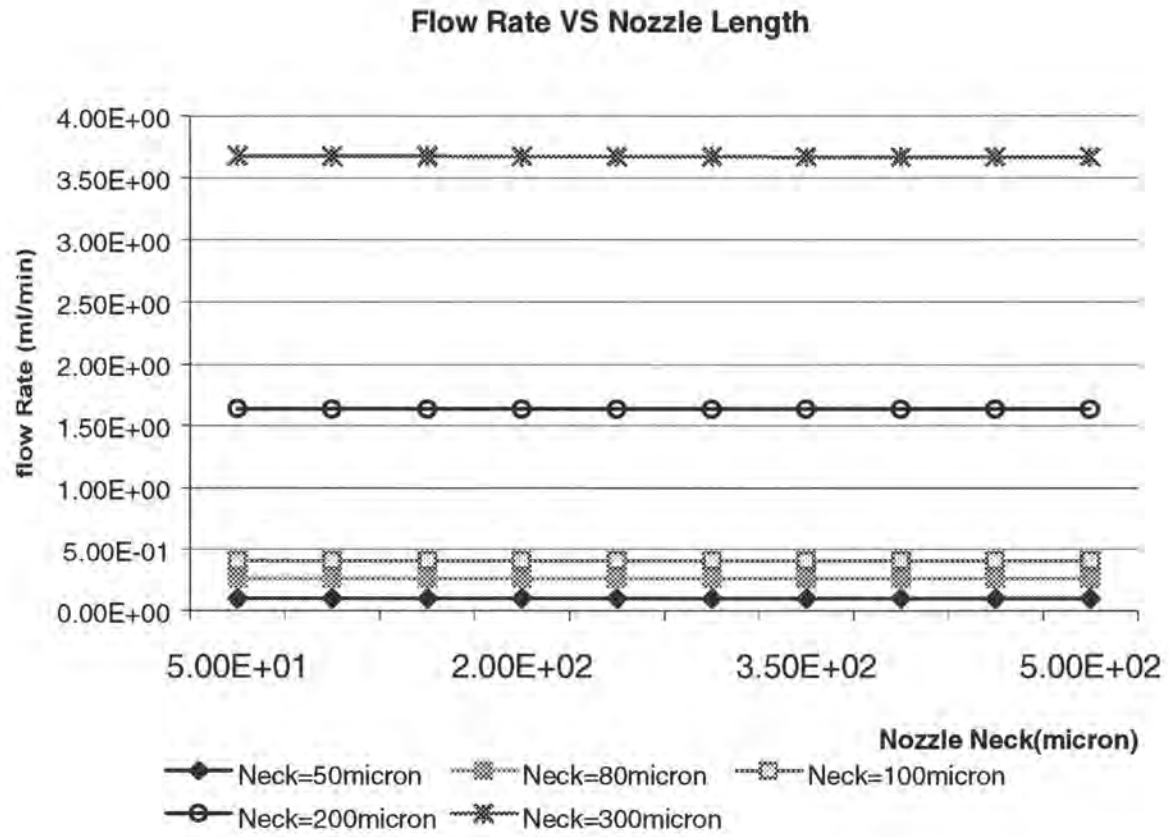


Figure 3.6 Effect of Nozzle Length on Flow Rate

3.3 Optimized Micropump

Micropumps are normally used in microsystem analysis to provide a certain flow rate and back pressure. We chose the membrane thickness as 500 microns, membrane radius as 25000 microns, nozzle neck as 80 microns and nozzle length as 400 microns. The choice of dimension is within the fabrication feasibility. Fig. 3.7 shows the optimized micropump performance at low frequency domain. Its working voltage is 50 V and working frequency is 50 HZ.

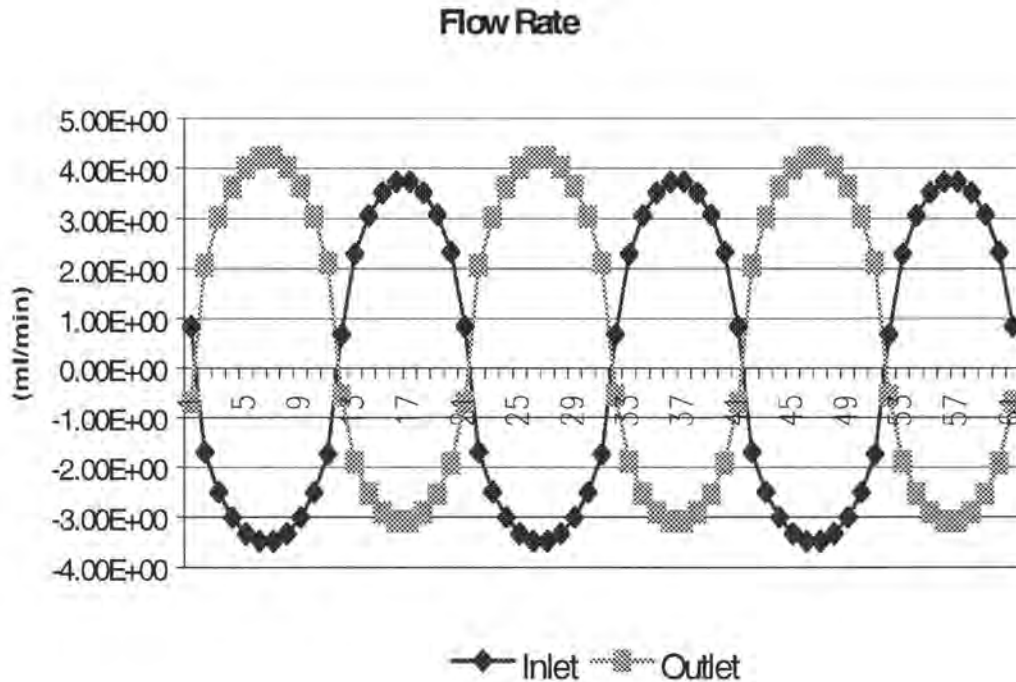


Figure 3.7 Optimized Micropump Inlet and Outlet Flow Rate

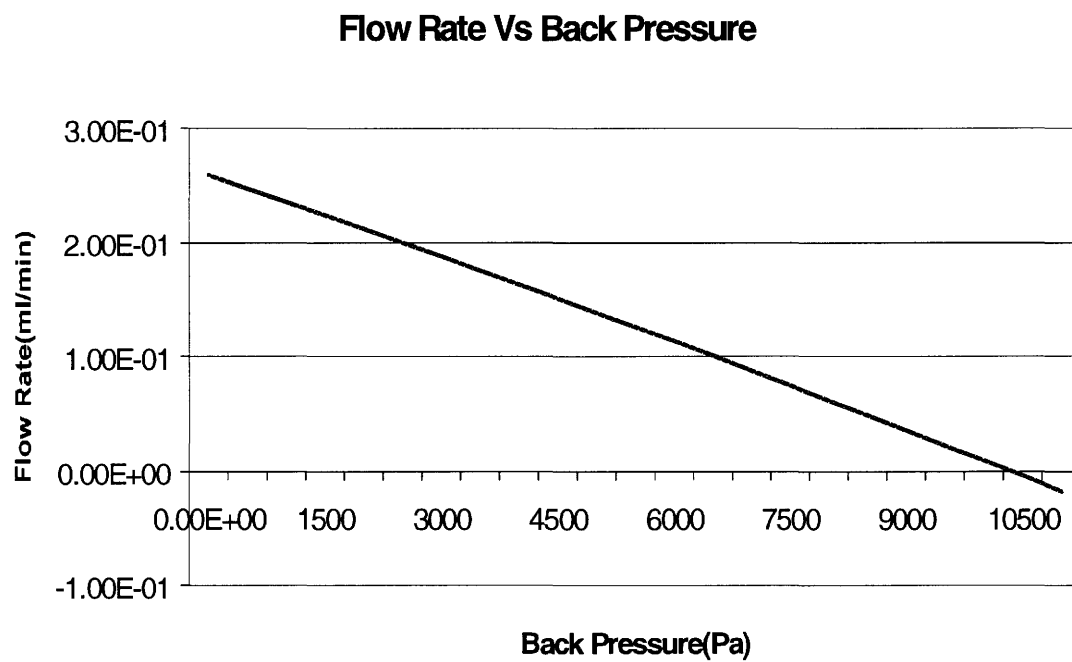


Figure 3.8 Optimized Micropump Working Characteristics

3.4 Performances in High Frequency Domain

The performance of a valveless micropump in a high frequency domain is also of great practical interest. When a micropump is working in high frequencies, of the order of millions of Hertz, the pressure rapidly changes its direction. At that time, flow inductivity is predominant and governs the fluid flow in the nozzle or diffuser. According to the discussions in Chapter 2, flow inductivity in the negative direction is less than that in the positive direction of the nozzle. But in low frequency domain, flow resistance plays a dominant role in the fluid flow. In this case, flow resistance in the negative direction is greater than that in the positive direction. Because of this different flow resistance, the net flow is from inlet to outlet. Whereas, at the millions of Hz of the working frequency, the flow inductivity governs the fluid flow inside the micropump. The flow inductivity in the positive direction is less than that in the negative direction. Because of this direction dependent flow inductivity, backflow will occur. In other words, the net flow will be from the outlet to the inlet.

Therefore, we can see that the micropump in a high frequency domain performs totally differently from the low frequency domain. One significant usage of this phenomenon is to control fluid flow direction inside a micropump by changing the working frequency. But unfortunately, PZT has its own working frequency range. Among these commercial PZT actuators, millions of HZ working frequency PZT actuators is not available now.

CHAPTER 4

FABRICATION OF VALVELESS MICROPUMP

In this chapter, mask design is discussed for different micropump dimensions. After the mask design, a fabrication process is developed based on the available facilities and experiment. Finally, problems encountered during the fabrication process are analyzed and discussed.

4.1 Mask Design of Micropump

Following the optimized micropump design presented in Chapter 3, the next step is to draw a set of masks for the device fabrication. Several commercial mask design software like L-edit and Cadence are available. In the Microelectronic Research Center (MRC) at Iowa State University, we used L-edit to draw masks.

Our micropump mask design consists of four layers: chamber layer, inlet layer, outlet layer, and a alignment mark layer. In order to compare the micropump performances with different pump dimensions, we chosen the deck dimension of inlet and outlet is chosen as 80 microns, 100 microns, 150 microns and 200 microns. Due to limited space, the diameter of the micropump chamber is chosen as 5 mm.

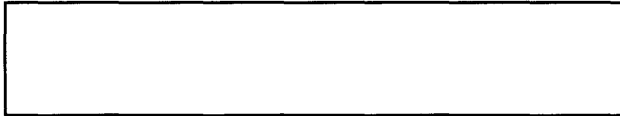
4.2 Fabrication of Micropump

The fabrication of the micropump was conducted in the Micro Technology Laboratory (MTL) at the University of Minnesota. After several experiments, the final fabrication process is developed as followings

A double polished 4" N type silicon wafer is RCA cleaned. Both sides were spin with positive PR 1818 around 2 microns. MAB6 microlithography with chamber mask (mask#1) was used for patterning the chamber and then hard baked on a hot plate for 1 minute. DRIE was used to etch the chamber for around 30 minutes to get a diameter of 5 mm and a depth of 80 microns. LPCVD was used to deposit 150-nm low stress nitride. MBA6 backside aligned inlet mask (mask#2) was used to open the inlet window and frontside aligned outlet mask (mask#3) to open the outlet window. Hard bake the wafer and use STS etcher to etch Nitride for 10 minutes. After that, acetone was used to strip the photo resists. The next step was the KOH (wt 49% 80 °C, around 16 hours) long time etching to etch through the whole wafer to form the inlet and outlet. After that, hot backflow phosphorus acid was used to strip the nitride. After finishing the silicon fabrication, a Pyrex 7740 wafer was bonded to the silicon wafer using anodic bonding to seal the micropump chamber. The final step is to stick a PZT disk on the glass membrane to serve as the actuator. The following is the detailed fabrication process.

A. Silicon Wafer

1.



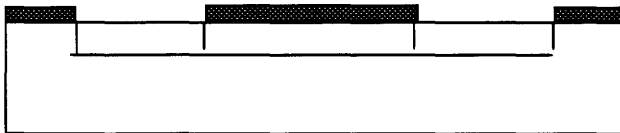
4" Silicon Wafer (100) N type RCA Clean

2.



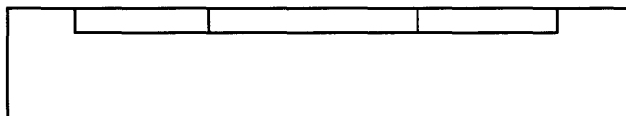
Spin PR1818 around 2 micron and photolithography define pattern with chamber mask
(Mask#1)

3.



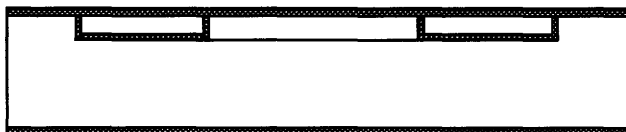
DRIE define pump Chamber and diffuser/Nozzle element with depth 80 micron

4.



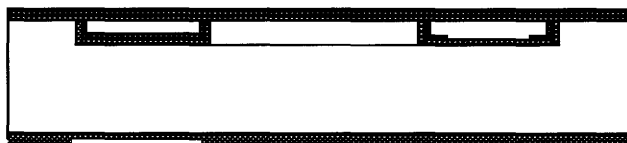
Strip PR with Acetone

5.



LPCVD Nitride both sides thickness 1500A

6.



Spin PR and pattern with backside alignment inlet mask (Mask#2) and front side alignment outlet mask (Mask#3)

7.



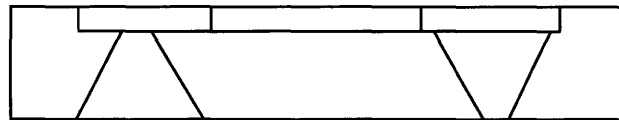
STS etcher opens LPCVD Nitride window and strip PR

8.



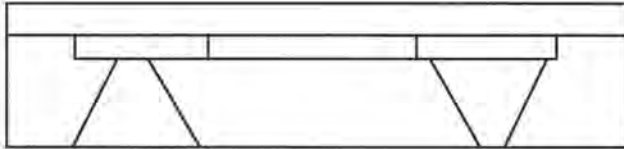
KOH 49% wt 80°C etch through as inlet and outlet

10.

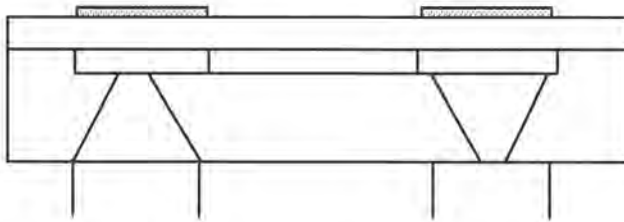


Phosphorous acid strip Nitride

B. Glass and Silicon anodic bonding



C. Stick PZT on the membrane with conductive epoxy.



4.3 Fabrication Problem Analysis

During the fabrication, several problems were observed including 350 °C PECVD nitride KOH etching strip and 400nm low stress nitride KOH etching strip. The two problems are analyzed as shown below.

4.3.1 350 °C PECVD Nitride KOH etching strip

KOH etching through the whole wafer normally takes a lot of time. The silicon nitride is often chosen as the mask material because the KOH etch rate of nitride is nearly zero. Therefore nitride is the ideal mask material for long time KOH etching. As the first experimental step, 350 °C PECVD Nitride is chosen. But after three hours KOH etching (wt 49% 80 °C), PECVD nitride was stripped increasingly.

The reason for this is that PECVD nitride has a porous property. Because of low deposition temperature, the deposit silicon nitride is not a dense material. The porous PECVD nitride is not enough to protect silicon from KOH for long time etching. Another reason is that PECVD step coverage is not as good as LPCVD. The PECVD nitride thickness in the chamber sidewall is much thinner on the surface and chamber bottom. For these reasons discussed above, it is better to choose LPCVD nitride mask material.

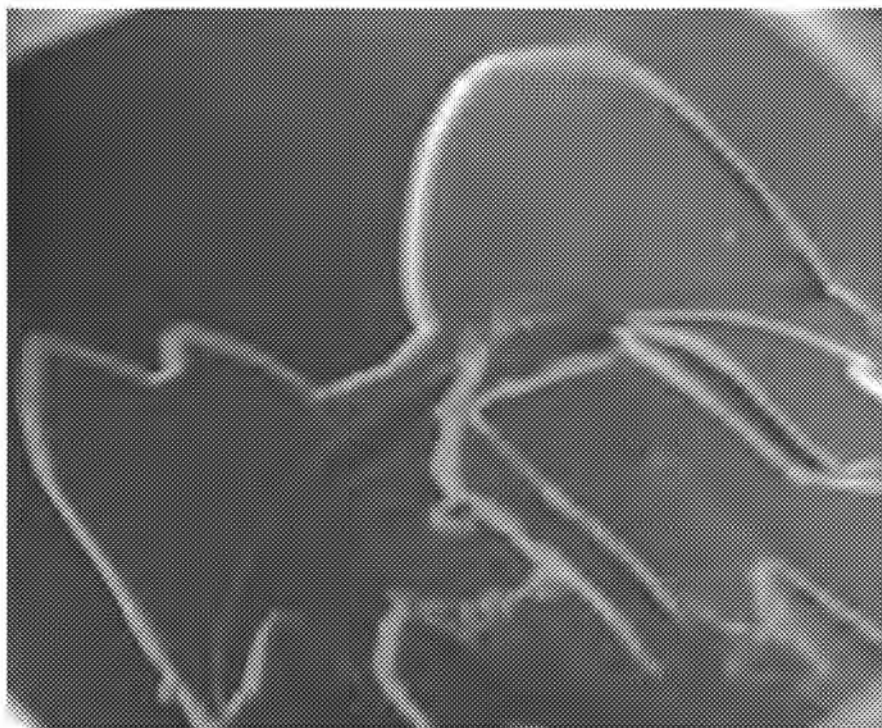


Figure 4.1 350°C PECVD Nitride KOH etching strip after 3 hours.

4.3.2 4000 Å low stress Nitride KOH etching strip

In MTL, 250 to 300 nm low stress nitride forms pinholes on the wafer surface after long time KOH etching. This may be due to the problems in STS etching. STS etcher opens the photoresist window while stripping the nitride away in some place, because of which, some pinholes can be formed. In the first experiment, a 400 nm-thickness low stress nitride is chosen as the KOH etching mask. But after six hours of etching, the 400 nm-thickness low stress nitride is also stripped. Figure 4.2 shows the 400 nm thick low stress nitride being stripped away after 6 hours of KOH etching.

The reason for this could be long deposition time and high deposition temperature. Although the nitride has a low stress, the long deposition time (20 hours) and the high deposit temperature will result in accumulated stress in the nitride. During KOH etching, H_2 bubbles collapse, and the surface tension strips off the high stress nitride. To solve this problem, one way is to reduce the silicon nitride thickness. Another way is to deposit an intermediate layer to reduce the accumulated stress in silicon nitride. For simplicity and feasibility, the first method is chosen in our fabrication.

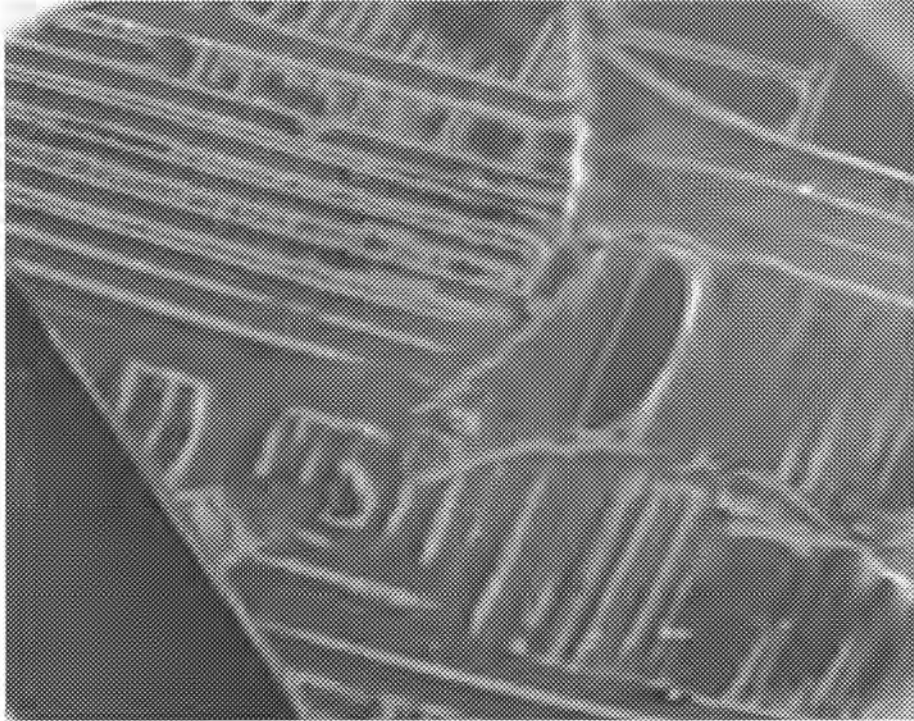


Figure 4.2 4000 A thickness low stress nitride strips away after 6 hours KOH etching.

CHAPTER 5

CONCLUSIONS

5.1 Conclusions of the present work

1. A dynamic model for the micropump is developed. At first, diffuser and nozzle direction dependent flow characteristics were analyzed. This model considers both solid mechanics and flow mechanics issues. The model can be used to predict the performance of the micropump under dynamic conditions.
2. Based on the dynamic model, micropump performance in low frequency domain was investigated. Several important parameters such as membrane dimension, nozzle dimensions were studied. In the low frequency domain, increasing the membrane thickness would not increase the flow rate and the backpressure. On the contrary, it will reduce the flow rate and backpressure. The flow rate increases with the nozzle neck dimension quadratically. For a small neck, the backpressure will increase with the nozzle neck. By increasing the nozzle neck to about 80 microns, the backpressure reaches its maximum. After that, the backpressure drops. When the neck dimension is bigger than 200 microns, the backpressure does not have any significant change. In the low frequency domain, neck length has little influence on back pressure and flow rate.
3. Following the modeling, a fabrication process was developed. Problems associated with the fabrication process was discovered and discussed. Information was used to revise the fabrication process.

5.2 Recommendation for future work

Future works for this project are followings:

1. Derive an accurate analytical PZT micropump membrane equation to describe the membrane performance. This analytical equation should include bonding material effect on the membrane performance.
2. Improve the micropump backpressure. In a microanalysis system, the fluid needs to go through the entire system. A typical pressure drop is around 20- 30 kpa. But the available PZT micropump backpressure is only 0.5 kpa. This is far less than what a microanalysis system requires. There are two ways to improve the micropump backpressure. One is to optimize the micropump design to get a higher backpressure the other way is to use a dual chamber design.
3. Study the micropump performance in a high frequency domain. In Chapter 3, this issue was briefly discussed. Since the flow inductivity in the high frequency domain plays a dominant role in micropump performance, the performance in the high working frequency will be totally different from the performance at the low working frequency. This also needs experimental verification.

REFERENCES

- Bardell, R. L., N. R. Sharma, F. K. Forster, M. A. Afroowitz and R. J. Penney, 1997, "Designing High performance micro-pumps based on no-moving-parts valves", *Proceedings of MEMS ASME*, 47-53
- Cao, L., S. Mantell and D. Polla, 2001, "Design and simulation of an implantable medical drug delivery system using microelectromechanical systems technology", *Sensors and Actuators A* 3084, 1-9
- Forster, F. K., R. L. Bardell, M. A. Afroowitz, N. R. Sharma and A. Blanchard, 1995, "Design, Fabrication and Testing of Fixed-Valve", *Proceedings of the ASME Fluids Engineering Division ASME*
- Francis, O., I. Dufour and E. Sarraute, 1997, "Analytical static modeling and optimization of electrostatic Micropumps", *Journal of Micromechanics & Microeng.* 7, 183-185.
Printed in the UK
- Gerlach, T., 1997, "Aspects of stationary and dynamic micro diffuser flow", *Transducer'97*, Chicago, June 16-19, 1035-1038
- Gerlach, T., and H. Wurmus, 1995, "Working principle and performance of the dynamic Micropump", *Sensors and Actuators A* 50, 135-140
- Gerlach, T., 1998, "Microdiffusers as dynamic passive valves for Micropump applications", *Sensors and Actuators A* 69, 181-191

- Gerlach, T., 1997, "Pumping Gases by a Silicon Micro Pump with Dynamic Passive Valves", *1997 International Conference on Solid-State Sensors and Actuators* Chicago, June 16-19
- Gong, Q. L., Z. Y. Zhou, Y. H. Yang and X. H. Wang, 2000, "Design, Optimization and Simulation on microelectromagnetic pump", *Sensors and Actuators A83*, 200-207
- Gravesen, P., J. Branebjerg and O. S. Jensen, 1993, "Microfluidics-a review", *Journal of Micromechanics & Microeng.* 3, 168-182. Printed in the UK
- Heschel, A., M. Mullenborn and S. Bouwstra, 1997, "Fabrication and Characterization of Truly 3-Diffuser/Nozzle Microstructures in Silicon", *Journal of Microelectromechanical systems* Vol. 6, No. 1
- Japikse, D. and N. C. Baines, 1998, "Diffuser design technology " Norwich, VT
- Jiang, X. N., Z. Y. Zhou, Y. Li, Y. Yang, X. Y. Huang and C. Y. Liu, 1997, "Experiments and Analysis for Micro-Nozzle/Diffuser flow and Micro Valveless Pumps", *1997 International Conference on Solid-State Sensors and Actuators* Chicago, June 16-19
- Koch, M., N. Harris, A. G. R Evans, N. M. White and A. Brunnschweiler, 1997, "A Novel Micromachined Pump Based On Thick-Film Piezoelectric Actuation", *International Conference on Solid-State Sensors and Actuators Chicago*, 1997 June 16-19
- Li, S.F., Y. Liu and S. C. Chen, 2001, "Dynamic Modeling and Optimization of Valve-less PZT Actuation Micropump", *Proceeding of Microfabrication and Micromachining*, San Francisco

- Makino, E., T. Mitsuya and T. Shibata, 2001, "Fabrication of TiNi shape memory micropump", *Sensors and Actuators A* 88, 256-262
- Meng, Q.Y., M. Mehregany and K. Deng, 1993, "Modeling of the electromechanical performance of piezoelectric laminated microactuators", *Journal of Micromechanics & Microeng.* 3, 18-23. Printed in the UK
- Morris, C. J., and F. K. Forster, 2000, "Optimization of a circular piezoelectric bimorph for a Micropump driver" *Journal of Micromechanics & Microeng.* 10, 2000, 459-465
- Nguye, N. T and R. M. White, 1999, "Design and optimization of an ultrasonic flexural plate wave micropump using numerical simulation", *Sensors and Actuators A* 77 229-236
- Olsson, A., G. Stemme and E. Stemme, 1999, "A numerical design study of the Valveless diffuser pump using a lumped-mass model", *Journal of Micromechanics & Microeng.* 9, 34-44
- Olsson, A., G. Stemme and E. Stemme, 2000, "Numerical and experimental studies of flat-walled diffuser elements for Valveless Micropump", *Sensors and Actuators A* 84, 165-175
- Olsson, A., G. Stemme and E. Stemme, 1995, "A valve-less planar fluid pump with two pump chambers", *Sensors and Actuators A* 46-47, 549-556
- Olsson, A., G. Stemme and E. Stemme, 1997, "Simulation studies of diffuser and nozzle elements for Valveless Micropump", *Transducer'97* Chicago, June 16-19, 1039-1042
- Olsson, A., P. Enoksson, G. Stemme and E. Stemme, 1997, "Micromachined flat-walled Valveless Diffuser Pumps", *Journal of Microelectromechanical Systems*, Vol., No. 2

- Olsson, A., P. Enoksson, G. Stemme and E. Stemme, 1996, "Diffuser-element design investigation for Valve-less pumps", *Sensors and Actuators A* 57, 137-143
- Olsson, A., P. Enoksson, G. Stemme and E. Stemme, 1996, "A valve-less planar pump isotropically etched in silicon", *Journal of Micromechanics & Microeng.* 6, 87-91.
Printed in the UK
- Pan, L. S., T. Y. Ng, G. R. Liu, K. Y. Lam and T. Y. Jiang, 2001, "Analytical solutions for the dynamic analysis of a valveless micropump-a fluid-membrane coupling study", *Sensors and Actuators A* 3052, 1-9
- Richter, M., R. Linnemann and P. Woias, 1998, "Robust design of gas and liquid Micropumps", *Sensors and Actuators A* 68, 480-486
- Saif, M. T. A., B. E. Alaca and H. Sehitoglu, 1999, "Analytical Modeling of Electrostatic Membrane Actuator for Micro Pumps", *Journal of Microelectromechanical systems* Vol. 8, No. 3
- Schneider, D. M., J. Maibach and E. Obermeier, 1995, "A New Analytical Solution for the Load-Deflection of Square Membranes", *Journal of Microelectromechanical systems* Vol. 4 No. 4
- Shah D K., S. P. Joshi and W. S. Chan, 1993, "Static structural response of plates with piezoceramic layer", *Smart Mater. Struct.* 2, 172-180. Printed in the UK
- Shoji, S. 1999. "Micro Total Analysis System (uTAS)", *Electronics and Communications in Japan Part 2* Vol. 82, No. 2, 385-393

- Shoji, S. and M. Esashi. 1993. "Microflow devices and systems", *Journal of Micromechanics & Microeng.* 4.157-171. Printed in the UK
- Stemme, E. and G. Stemme, 1993, "A Valveless diffuser/nozzle-based fluid pump", *Sensors and Actuators, A* 39, 159-167
- Timoshenko, S. and S. Woinowsky-Krieger, 1995, "Theory of Plates and Shells" Second Edition McGraw-Hill.
- Ullmann, A., 1998, "The piezoelectric valve-less pump-performance enhancement analysis", *Sensors and Actuators A* 69, 97-105
- Ulrich, J., H. Fuller and R. Zengerle, 1995, "Static and Dynamics Flow Simulation of a KOH-Etched Micro Valve", *The 8th international Conference on Solid-State Sensors and Actuators, and Eurosensors IX*, Stockholm, Sweden
- Wang, X. H., Z. Y. Zhou, X. Y. Ye, Y. Li, and W. D. Zhang, 1998, "A PZT-driven Micropump" *International Symposium on Micromechatronics and Human Science*
- White, F. M., 1991, "Viscous Fluid Flow" Second Edition McGraw-Hill, Inc
- Xu, D., L. Wang, G. F. Ding, Y. Zhou, A. B. Yu and B. C. Cai, 2001, "Characteristics and fabrication of NiTi/Si diaphragm micropump", *Sensors and Actuators A* 3045, 1-6
- Yu, J. C. and C. B. Lan, 2001, "System modeling of microaccelerometer using piezoelectric thin films", *Sensors and Actuators A* 88, 178-186
- Zengerle, R. and M. Richter, 1993, "Simulation of Microfluid systems", *Journal of Micromechanics & Microeng.* 4, 192-204. Printed in the UK

Zengerle, R., W.Geiger, M.Richter, J.Ulrich, S.Kluge and A.Richter, 1995 "Transient measurements on miniaturized diaphragm pumps in microfluid systems" *Sensors and Actuators A*46-47, 557-561